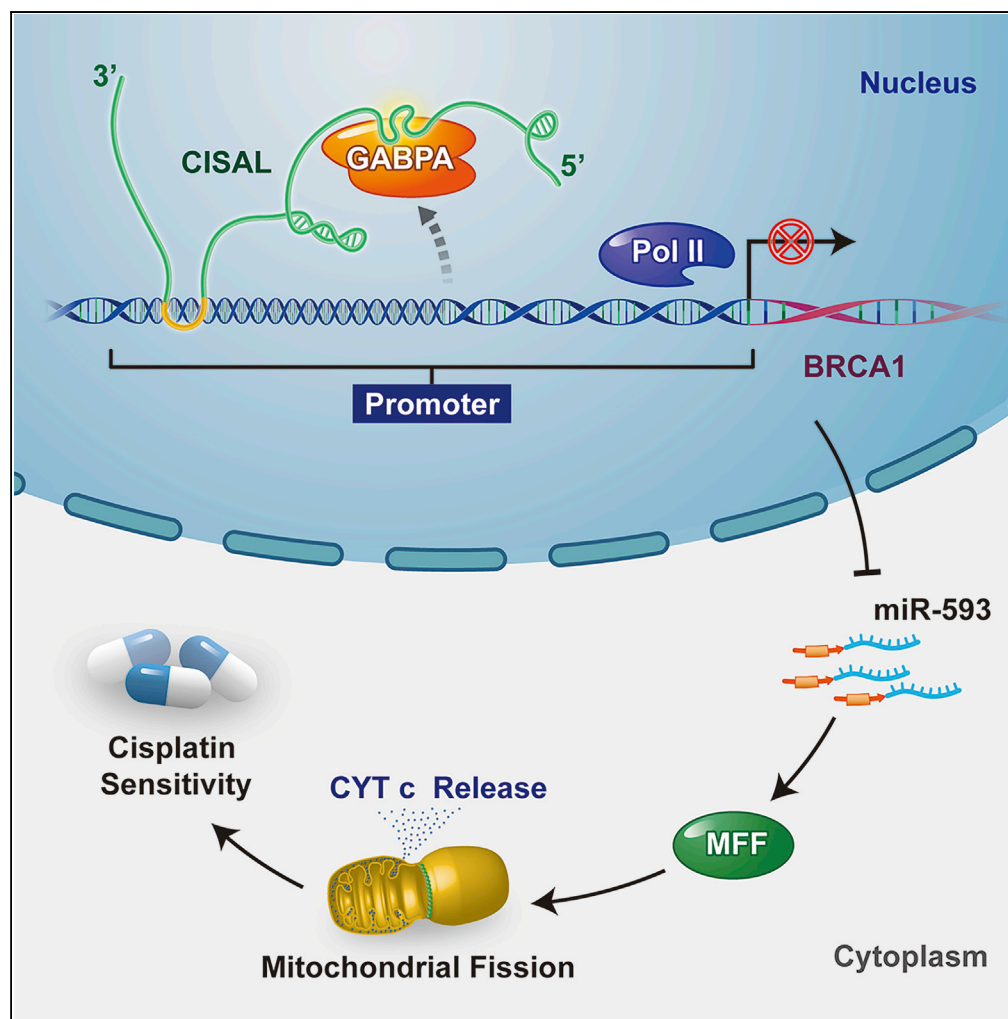## Article

lncRNA CISAL Inhibits BRCA1 Transcription by Forming a Tertiary Structure at Its Promoter

Song Fan, Tian Tian, Xiaobin Lv, ..., Dechen Lin, Bakhos A. Tannous, Jinsong Li

fansong2@mail.sysu.edu.cn (S.F.)
rysyshospital@163.com (Y.R.)
lijins@mail.sysu.edu.cn (J.L.)

HIGHLIGHTS

CISAL enhances mitochondrial fission and cisplatin sensitivity in TSCC cells through BRCA1

CISAL directly binds the BRCA1 promoter and forms an RNA-DNA triplex structure

CISAL sequesters GABPA away from regulatory binding at BRCA1 promoter

High CISAL predicts favorable neoadjuvant chemosensitivity and prognosis of TSCC patients

CellPress

Article

lncRNA CISAL Inhibits BRCA1 Transcription by Forming a Tertiary Structure at Its Promoter

Song Fan,[1,2,13,14,*] Tian Tian,[3,13] Xiaobin Lv,[4,13] Xinyuan Lei,[1,5,13] Zhaohui Yang,[2] Mo Liu,[1] Faya Liang,[1] Shunrong Li,[1] Xiaofeng Lin,[1] Zhaoyu Lin,[1] Shule Xie,[1] Bowen Li,[2] Weixiong Chen,[2,6] Guokai Pan,[2] Xinyu Lin,[1] Zhanpeng Ou,[1] Yin Zhang,[1] Yu Peng,[1] Liping Xiao,[1] Lizao Zhang,[1] Sheng Sun,[7] Hanqing Zhang,[1] Sigeng Lin,[8] Qunxing Li,[1] Binghui Zeng,[9] Filippos Kontos,[10] Yi Ruan,[11,*] Soldano Ferrone,[10] Dechen Lin,[1] Bakhos A. Tannous,[12] and Jinsong Li[1,2,*]

SUMMARY

Cisplatin-based neoadjuvant chemotherapy has been shown to improve survival in patients with squamous cell carcinoma (SCC), but clinical biomarkers to predict chemosensitivity remain elusive. Here, we show the long noncoding RNA (lncRNA) LINC01011, which we termed cisplatin-sensitivity-associated lncRNA (CISAL), controls mitochondrial fission and cisplatin sensitivity by inhibiting BRCA1 transcription in tongue SCC (TSCC) models. Mechanistically, we found CISAL directly binds the BRCA1 promoter and forms an RNA-DNA triplex structure, sequestering BRCA1 transcription factor-GABPA away from the downstream regulatory binding region. Importantly, the clinical relevance of these findings is suggested by the significant association of CISAL and BRCA1 expression levels in TSCC tumors with neoadjuvant chemosensitivity and overall survival. We propose a new model where lncRNAs are tethered at gene promoter by RNA-DNA triplex formation, spatially sequestering transcription factors away from DNA-binding sites. Our study uncovers the potential of CISAL-BRCA1 signaling as a potential target to predict or improve chemosensitivity.

INTRODUCTION

Around 70% of the human genome is transcribed to RNA, whereas only 2% consists of protein-coding genes (Ulitsky and Bartel, 2013). The many noncoding RNA (ncRNA) loci interdigitate between, within, and among protein-coding genes on both strands. In addition to miRNAs, recent studies suggest that long noncoding RNAs (lncRNAs), >200 nucleotides (nt), are expressed at lower levels than protein-coding transcripts and are more tissue specific (Cabili et al., 2011; Derrien et al., 2012). Further, lncRNAs can serve as scaffolds or guides to regulate protein-protein or protein-DNA interactions as decoys to bind proteins or microRNAs (miRNAs) and as enhancers to influence gene transcription when transcribed from enhancer regions (enhancer RNA) or their neighboring loci (ncRNA activator) (Hu et al., 2014). These lncRNAs have emerged as key regulators of important biological processes implicated in cell proliferation (Bian et al., 2018), differentiation (Russell et al., 2015), migration (Wang et al., 2017), immune response (Heward and Lindsay, 2014), and apoptosis in various cancer types, acting as tumor suppressors or oncogenes (Liu et al., 2018; Xing et al., 2018).

Mechanistically, recent studies revealed that a subset of lncRNAs regulate gene expression in *cis* and in *trans* by interacting with chromatin and recruiting chromatin modifiers (Bonasio and Shiekhattar, 2014; Carpenter et al., 2013). LncRNAs can function at their sites of synthesis to regulate local gene expression using either RNA-dependent (Lam et al., 2013) or RNA-independent mechanisms (Hah et al., 2013). A small but growing number of lncRNAs have been shown to positively regulate the expression of neighboring protein-coding genes on the same chromosome by altering local chromatin accessibility and/or structure (Lam et al., 2013; Melo et al., 2013). Furthermore, genomic binding profiles showed that a single lncRNA transcript can interact with multiple binding sites on different chromosomes away from its site of transcription (Rinn et al., 2007). Long-range intrachromosomal interactions between lncRNA-expressing loci and distant loci have also been documented (Hacisuleyman et al., 2014; Li et al., 2013). Although lncRNA can have dual functions, both acting locally to regulate the expression of its neighboring protein-coding gene and distally at regulatory elements genome-wide, the activity of lncRNAs depends largely on protein partners, such as transcription factors (TFs) or histones. Some studies suggested that lncRNAs could spatially correlate with

[1]Guangdong Provincial Key Laboratory of Malignant Tumor Epigenetics and Gene Regulation of Sun Yat-Sen Memorial Hospital, Guangzhou 510120, China

[2]Department of Oral and Maxillofacial Surgery, Sun Yat-Sen Memorial Hospital of Sun Yat-Sen University, Guangzhou 510120, China

[3]Department of Neurobiology, Key Laboratory of Human Functional Genomics of Jiangsu, Nanjing Medical University, Nanjing, Jiangsu 211166, China

[4]Nanchang Key Laboratory of Cancer Pathogenesis and Translational Research, Center Laboratory, the Third Affiliated Hospital, Nanchang University, Nanchang 330047, China

[5]State University of New York at Stony Brook, Stony Brook, NY 11794, USA

[6]Department of Stomatology, Longgang Distric Central Hospital, Affliated to Guangzhou University of Traditional Chinese Medicine, Shenzhen, Guangdong 518116, China

[7]Massachusetts General Hospital Cancer Center, Harvard Medical School, Boston, MA 02114, USA

[8]Department of Oral and Maxillofacial Surgery, Hainan General Hospital, Hainan 570300, China

[9]Guanghua School of Stomatology, Hospital of Stomatology, Guangdong Provincial Key Laboratory of Stomatology, Sun Yat-sen

TFs across the genome (Herriges et al., 2014), whereas others showed that lncRNAs appear to inhibit DNA binding of their associated TFs at several target sites (Sun et al., 2013). In any case, the direct interaction of lncRNA-DNA triplex and TFs remains unclear.

Recent studies revealed that an abnormal mitochondrial dynamic participates in the regulation of apoptosis (Suen et al., 2008) and is linked to a variety of diseases including cancer (Wang et al., 2011). Cisplatin has been heavily employed as a cornerstone treatment in the fight against a wide spectrum of solid neoplasms over the past 30 years. However, chemoresistance frequently develops and leads to therapeutic failure. The initial patient responsiveness to platinum-based therapies in oral squamous cell carcinoma (OSCC) is 80.6% (Zhong et al., 2013); however, more than 70% of patients eventually relapse due to tumor-acquired resistance (Gibson et al., 2005). Numerous studies tried to unravel the mechanism responsible for cisplatin resistance, but no substantive progress has been made to date to overcome this resistance. Here, we investigated the role of lncRNAs in regulating mitochondrial fission and cisplatin sensitivity in tongue squamous cell carcinoma (TSCC). We identified CISAL as one key lncRNA that participates in this process. Moreover, we show that CISAL can directly form an RNA–DNA triplex structure at the BRCA1 promoter and inhibit BRCA1 transcription activity by sequestering TF-GABPA away from its DNA-binding sites. Our data reveal a new role of lncRNAs in transcriptional regulation by expanding the known functions of the lncRNA-BRCA1 signaling axis in the mitochondrial network and chemosensitivity.

RESULTS

Differential Expression of lncRNAs Induced by Cisplatin in TSCC Cells and Tumor Tissues

Recent studies have demonstrated that lncRNAs play pivotal roles in regulating the biological properties of cancer (Peng et al., 2017). Previously, we showed that mitochondrial fission determines cisplatin sensitivity in tongue squamous cell carcinoma (TSCC) (Fan et al., 2015a, 2015b). We wonder whether lncRNAs participate in this chemosensitivity program in TSCC. We first profiled the expression of lncRNAs in two TSCC cell lines (CAL-27 and SCC-9) under cisplatin treatment in comparison to their matched untreated controls using microArray. A total of 1,266 upregulated lncRNAs and 2,432 downregulated lncRNAs with significant differential expression (fold change ≥ 2) were found in CAL-27 cells, whereas SCC-9 cells showed 2,951 upregulated and 3,312 downregulated lncRNAs (Figure 1A). When we increased the cut-off for differentially expressed lncRNAs to ≥ 4, we found 38 upregulated lncRNAs (Figure 1B) and 143 downregulated lncRNAs (Figure S1A) under cisplatin treatment in both cell lines compared with their untreated parental controls. We then focused on these 38 upregulated lncRNAs and confirmed their expression levels in TSCC cells using qRT-PCR (Figure S1B). We also obtained matched pre- and post-cisplatin-treated TSCC tumor tissues from patients with chemosensitive and chemoresistant tumors (Table S1) and analyzed them for these lncRNA by qRT-PCR. Among the 38 lncRNAs, we found 19 of them to be highly upregulated in chemosensitive TSCC tumors before neoadjuvant chemotherapy as compared with chemoresistant tumors (Figure S1C) (fold change ≥ 2). On the other hand, 13 lncRNAs were confirmed to be significantly upregulated in chemosensitive tumors, as compared with their matched pre-treated tumors as well as chemoresistant tumors (Figure 1C). Notably, one lncRNA (RefSeq accession number LINC01011) was mostly upregulated in chemosensitive tumors (Figures 1C and S1C). Thus, we focused on this uncharacterized lncRNA and named it CISAL (cisplatin sensitivity-associated lncRNA). We first confirmed that CISAL is located on chromosome 6 in humans and composed of three exons with a full length of 1583 nt by rapid amplification of cDNA ends (RACE) in the CAL-27 cell line (Figures 1D and S2A, and Table S2). The non-coding nature of CISAL was confirmed by coding-potential analysis (Figures S2B and S2 C). Expression of CISAL, further determined by locked nucleic acid (LNA)-based *in situ* hybridization (ISH), was markedly increased in patients with neoadjuvant chemosensitive tumors and was mainly localized to the nucleus (Figures 1E and 1F). The specificity of CISAL probes was confirmed as shown in Figures S3A–S3D.

CISAL Regulates the Mitochondrial Fission and Cisplatin Sensitivity in TSCC

We tested whether CISAL could regulate mitochondrial fission and cisplatin sensitivity in TSCC cells. CISAL knockdown by shRNA attenuated mitochondrial fission and cell apoptosis upon cisplatin treatment in TSCC cells (Figures 2A, 2B, S3E, and S3F). Moreover, the release of cytochrome c (CYT c) from the intermembrane space of the mitochondria to the cytosol and caspase-3/7 activity were attenuated upon CISAL silencing in TSCC cells under cisplatin treatment (Figures 2A and S3G). In contrast, mitochondrial fission and apoptosis were increased by enhanced CISAL expression (Figures S3H–S3J). Meanwhile, overexpression of CISAL abolished the inhibitory effect of CISAL knockdown on mitochondrial fission and apoptosis, excluding the possibility that the inhibitory effect was affected by off-target effect of CISAL

University, Guangzhou 510055, China

[10]Department of Surgery, Massachusetts General Hospital, Harvard Medical School, 55 Fruit Street, Boston, MA 02114, USA

[11]Department of Oral Medicine, Sun Yat-Sen Memorial Hospital of Sun Yat-Sen University, Guangzhou 510120, China

[12]Experimental Therapeutics and Molecular Imaging Lab, Department of Neurology, Massachusetts General Hospital and Harvard Medical School, Boston, MA 02129, USA

[13]These authors contributed equally

[14]Lead Contact

*Correspondence:
fansong2@mail.sysu.edu.cn (S.F.),
rysyshospital@163.com (Y.R.),
lijins@mail.sysu.edu.cn (J.L.)
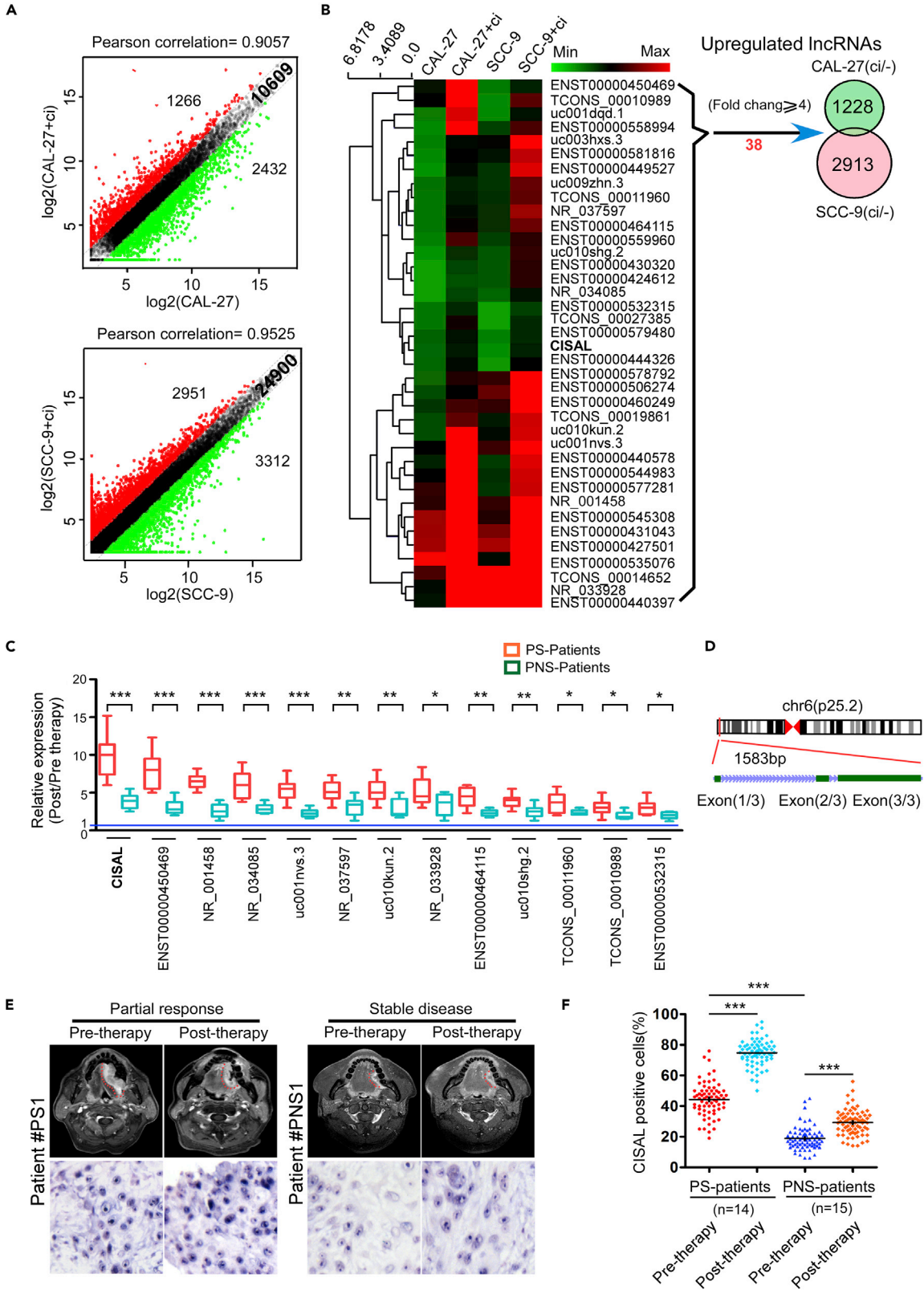
https://doi.org/10.1016/j.isci.
2020.100835

Figure 1. Differential Expression of lncRNAs Induced by Cisplatin in TSCC Cells and Chemosensitive or Chemoresistant Tumors

(A) Scatterplot showing variation in lncRNA expression between treated and non-treated TSCC cells. The values on the X- and Yaxes are the average normalized signal values of the group (log2 scaled). The green and red dots represent fold change ≥2.0.

(B) Heatmap showing 38 upregulated lncRNAs in both treated TSCC cell lines compared with the untreated cells. The relative lncRNA expression is depicted according to the color scale. Venn diagram of the intersection of the upregulated lncRNAs in both treated TSCC cell lines versus the untreated cells. Thirty-eight lncRNAs showed a fold change ≥4.0.

(C) Thirteen lncRNAs were identified to be significantly upregulated in TSCC tumors with chemosensitive (PS) and chemoresistant tumors (PNS).

(D) Schematic annotation of the CISAL genomic locus on chr6:2,988,648-2,991,173 in humans. Green rectangles represent exons.

(E) Representative MRI scans of tumor response (upper panels) and CISAL expression (lower panels) in tissue specimens from patient with chemosensitive and chemoresistant TSCC tumors.

(F) CISAL expression in each patient was analyzed by *in situ* hybridization; 5×200 tumor cells were randomly counted in each tumor.

*$p < 0.05$, **$p < 0.01$, and ***$p < 0.001$ versus control, (C) 2-tailed Student's t test; (F) 1-way ANOVA followed by Dunnett's tests for multiple comparisons.

siRNAs (Figures S3K and S3L). Further, we wondered whether the upregulation of CISAL expression is only prevalent in cisplatin-treated cells. As expected, adriamycin (ADR) and camptothecin (CPT) did not have any effect on CISAL expression in two TSCC cells (Figure S3M). Interestingly, TCGA database analysis showed that higher expression of CISAL correlated with better prognosis in multiple types of human cancer, including bladder carcinoma, low-grade glioma, lung adenocarcinoma, ovarian cancer, and pancreatic adenocarcinoma, further supporting the tumor suppressor role of CISAL in human cancer (Figure S4).

CISAL Regulates Mitochondrial Fission and Cisplatin Sensitivity Through BRCA1

Recent studies have suggested that lncRNAs have regulatory roles in the transcriptional control of protein-coding genes both in *cis* and in *trans*, and the number of known lncRNA functions is growing rapidly (Carpenter et al., 2013). To explore the downstream target genes of lncRNAs involved in regulating mitochondrial fission and cisplatin sensitivity in TSCC cells, we used RNA profiling technology to simultaneously analyze the mRNA expression levels of genes that were differentially regulated by CISAL. In cisplatin-treated cells, silencing of CISAL by two different shRNAs (shCISAL2 and shCISAL5) led to upregulation of 523 genes, whereas 348 genes were downregulated in both the CAL-27 and SCC-9 cell lines (fold change ≥2) (Figure 2C). Gene set enrichment analysis (GSEA) (Subramanian et al., 2005) identified five and three significantly activated pathways for upregulated and downregulated genes, respectively (Figures 2D and S5A). Of these genes, BRCA1 was the most prominent in response to DNA damage, DNA repair, and double-strand break repair pathways (Figure 2D). Cisplatin is known to induce proapoptotic effect by damaging DNA (Hu et al., 2016), and BRCA1 plays a crucial role in the DNA damage response (Schrock et al., 2017). Our previous study also revealed that BRCA1 transactivates miR-593-5p expression and downregulates MFF to attenuate cisplatin sensitivity and mitochondrial fission in TSCC cells (Fan et al., 2015b). Thus, we hypothesized that CISAL knockdown attenuates mitochondrial fission and TSCC cell apoptosis upon cisplatin treatment potentially through regulating BRCA1 expression. Indeed, CISAL knockdown led to a significant increase in BRCA1 levels under cisplatin treatment, and downstream genes of BRCA1, including miR-593 and MFF (Fan et al., 2015b), were upregulated and decreased, respectively (Figures S5B–S5D). In contrast, overexpression of CISAL induced a reverse effect (Figures S5E–S5G). These data suggest that BRCA1 is a downstream target gene of CISAL. To confirm the association of CISAL and BRCA1 in regulating mitochondrial fission and cisplatin sensitivity, we used shRNA to knockdown BRCA1 expression and observed that the inhibitory effect of CISAL knockdown on mitochondrial fission and apoptosis under cisplatin treatment was attenuated by BRCA1 silencing (Figures 2E, 2F, S5H, and S5I). Meanwhile, BRCA1 mRNA levels were also confirmed by qRT-PCR (Figure S5J). All together, these data suggest that CISAL mediates mitochondrial fission and cisplatin sensitivity in TSCC cells by regulating BRCA1 expression. Notably, TCGA analysis showed that lower expression of BRCA1 correlates with good prognosis in multiple types of human cancer, including bladder carcinoma, lower-grade glioma, lung adenocarcinoma, pancreatic adenocarcinoma, invasive breast carcinoma, papillary renal cell carcinoma, and head neck squamous cell carcinoma (Figure S6), further supporting the clinical relevance of BRCA1 signaling pathway.

CISAL Directly Binds to BRCA1 Promoter and Forms RNA–DNA Triplex Structure

We next aimed to address the important question of how CISAL targets BRCA1 in *trans*. Study of genomic association showed that lncRNAs can interact with gene promoters by forming RNA–DNA triplex, possibly through Hoogsteen base pairing, to regulate the target gene expression (Mondal et al., 2015). To explore potential lncRNA-binding sites within the BRCA1 promoter, we calculated the binding potential of CISAL to fragments covering 2000 bp upstream and 200 bp downstream of the transcriptional start sites (TSSs) of BRCA1 and GAPDH (control) by IntaRNA. The heatmap revealed a short stretch in the CISAL RNA that was
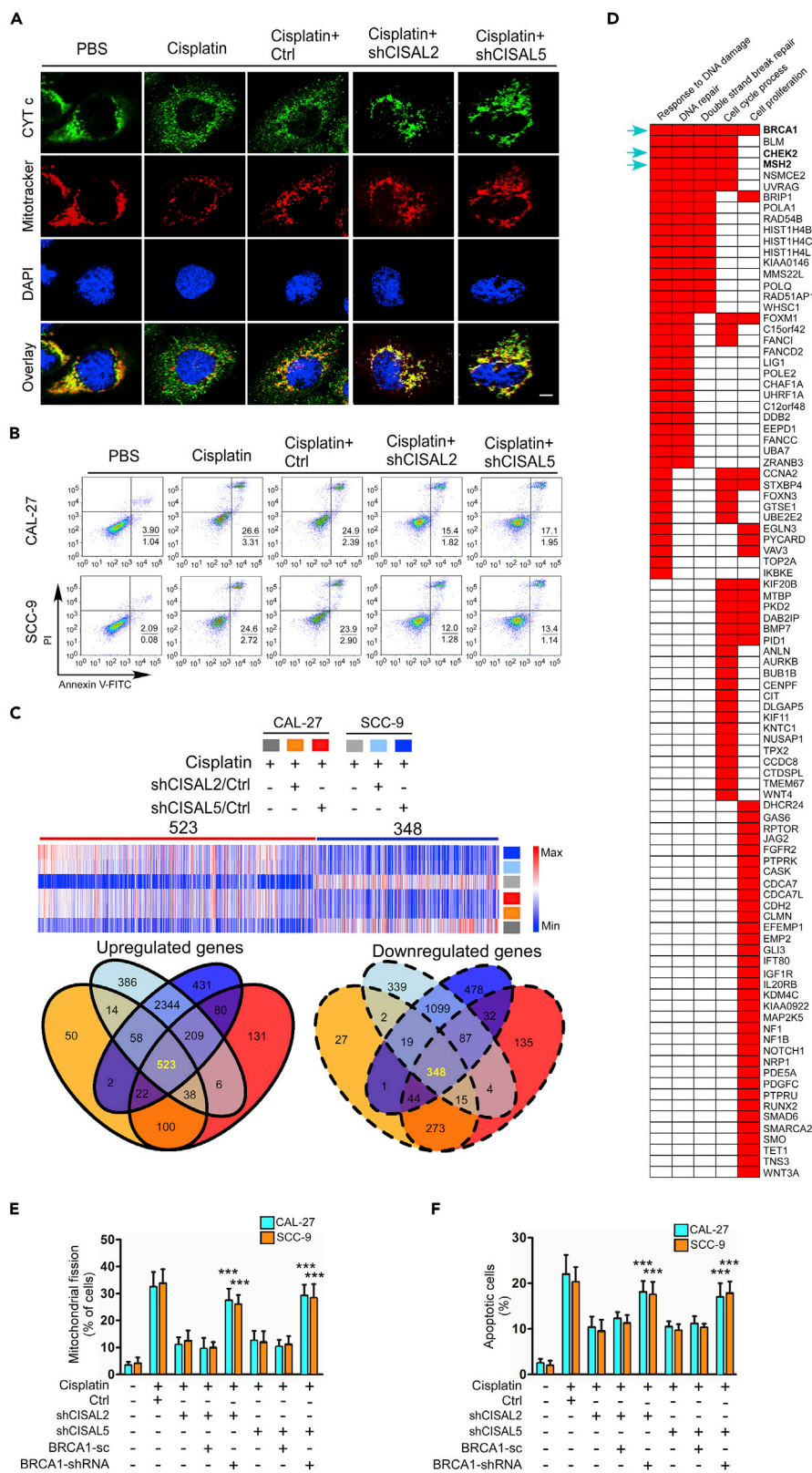
Figure 2. CISAL Promotes Mitochondrial Fission and Cisplatin Sensitivity in TSCC Cells through BRCA1

(A and B) CAL-27 and SCC-9 cells were treated with shRNA against CISAL. Mitochondrial fission and CYT c distribution was detected by staining with MitoTracker Red and antibodies against CYT c, respectively (A); cell apoptosis was detected using flow cytometry (B).

(C) CAL-27 and SCC-9 cells stably expressing two different shRNAs against CISAL (shCISAL2 and shCISAL5) were treated with cisplatin and their RNA was extracted and analyzed for mRNA profiling. Heatmap (upper panel) and Venn diagrams (lower panel) depict differentially expressed mRNAs in cisplatin-treated cells stably expressing shCISAL (fold change ≥2.0). Blue to red color gradation is based on the ranking of each condition from minimum (blue) to maximum (red).

(D) Gene set enrichment analysis (GSEA) showing five significantly induced pathways related to the genes upregulated in response to CISAL knockdown in both TSCC cell lines under cisplatin treatment.

(E and F) The inhibitory effect of CISAL knockdown on mitochondrial fission, analyzed by staining with MitoTracker red (E), and apoptosis using flow cytometry (F), after BRCA1 silencing.

***p<0.001, 2-tailed Student's t test. Data are represented as mean ±SEM.

predicted to bind to a complementary region in the BRCA1 promoter at (−1627, −1606), whereas the GAPDH promoter was negative throughout the region (Figures 3A and 3B).

To investigate the interaction of CISAL and BRCA1 regulation, we evaluated their subcellular location. Northern blotting and RNA fluorescence *in situ* hybridization (Kim et al., 2015) showed that substantial amounts of CISAL were mainly visible in the nucleus in CAL-27 cells (Figure 3C), consistent with the results from TSCC tissues (Figure 1E). We also found that localization of CISAL was not significantly changed upon cisplatin treatment or overexpression of CISAL (Figures S7A and S7B). To experimentally examine whether the predicted CISAL matching sequences have the potential to form a triple-stranded structure with the BRCA1 promoter, we incubated biotin-labeled DNA fragments (BRCA1-70, 70 nt) with tiled 20 nt RNA oligonucleotides and analyzed the formation of RNA-DNA triplexes by electrophoretic mobility shift assay (EMSA) (Figure 3D). The oligoribonucleotide sequence (oligo #4) retarded the mobility of the DNA fragment, unlike any other oligos, suggesting that oligo #4 interacts with the DNA, presumably by forming a triplex structure with the predicted sequence. On the other hand, treatment with RNase H did not affect the mobility of the RNA-DNA complex, ruling out the possibility that the shift in electrophoretic mobility is due to the formation of DNA-RNA heteroduplexes (Figure 3E). Again, no triplex formation was observed with mutant oligo (Figure 3E), reinforcing the necessity for a specific sequence between lncRNA and DNA to form triplex structures. We also examined whether CISAL could bind to the chromatin of the regulatory regions of BRCA1 and GAPDH genes by performing a chromatin isolation using RNA purification (ChIRP) assay. The cross-linked CAL-27 cell lysates were incubated with biotinylated DNA probes against CISAL, and the binding complexes were recovered using streptavidin-conjugated magnet beads. Enrichment of the specific regulatory regions of BRCA1, but not of the unrelated region or GAPDH gene, by CISAL was detected (Figure 3F). Moreover, cisplatin treatment enriched CISAL-binding regions at BRCA1 promoter as demonstrated by a ChIRP assay (Figure S7C). Interestingly, lncRNA NBR2 has been fairly well studied (Liu et al., 2016), and CISAL triplex can actually form in the region within the first intron of lncRNA NBR2. Taking that into consideration, we investigated whether regulation of CISAL expression had any effect on lncRNA NBR2 expression level. Our data revealed that lncRNA NBR2 expression level was not affected by CISAL overexpression/knockdown (Figures S7D and S7E). Taken together, these results suggest that CISAL might be recruited to the specific regulatory region of BRCA1 and form triplex structures.

CISAL Facilitates Transcriptional Repression by Counteracting GABPA Binding with BRCA1 Promoter

We evaluated how the interaction of CISAL and BRCA1 promoter inhibits BRCA1 expression. Recent discoveries demonstrated that the cellular localization of lncRNAs is informative regarding its function, whereas nuclear lncRNAs could plausibly have functions in histone modification (Greco and Condorelli, 2015) or direct transcriptional regulation (Long et al., 2017). Therefore, we first sought to determine whether CISAL regulates BRCA1 via histone methylation or acetylation. ChIP assays showed that CISAL overexpression or silencing had no effect on H3 methylation or H3/H4 acetylation of the promoter of BRCA1 (Figures S8A–S8D). Moreover, inhibitory efficacy of CISAL overexpression on BRCA1 expression was comparable between CAL-27 and SCC-9 cells under the treatment of AZA/TSA or PBS (Figures S8E and S8F). Hence, it is most likely that CISAL-mediated BRCA1 expression is not regulated by the "first hit"—histone modification.

During the last decade, investigation has uncovered that many lncRNAs can actively modulate the DNA-binding activity of their associated TFs by acting as non-DNA binding cofactors (Rapicavoli et al., 2011).
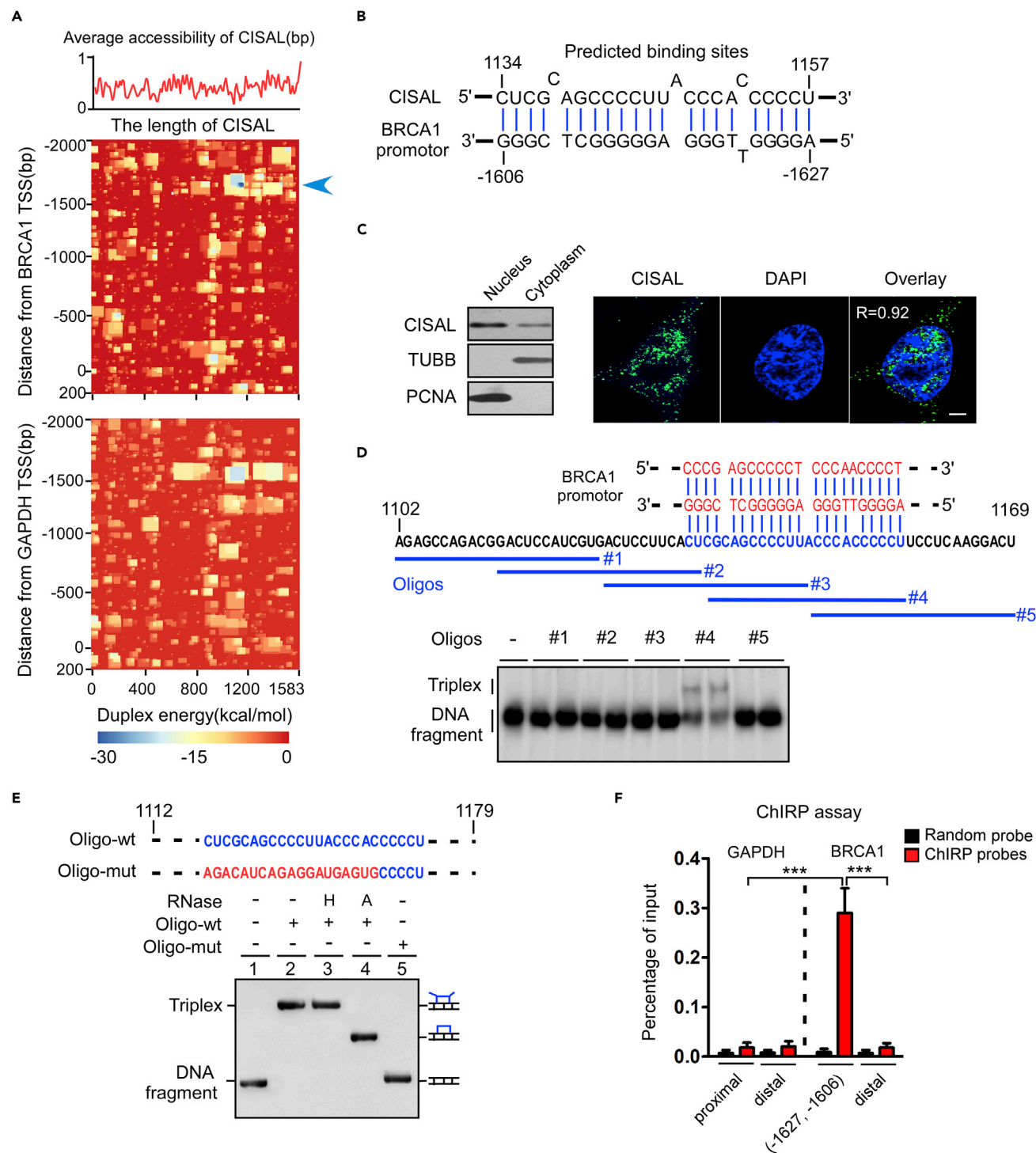
Figure 3. CISAL Forms DNA: RNA Triplex Structure with the BRCA1 Promoter

(A) Binding potential between CISAL and BRCA1 or GAPDH promoter regions using IntaRNA. The red curve shows the average probability of single-stranded RNA. Heatmap represents the base-pairing energy for an RNA/RNA duplex model for seed-based regions along the CISAL transcript and 2,000 bp upstream and 200 bp downstream of the TSS of BRCA1 (upper) and GAPDH (lower).

(B) Representation of the predicted interaction of CISAL sequence and the promoter DNA region of BRCA1 at the lowest free energy loci.

(C) Northern blotting (left panel) and FISH (right panel) revealing that CISAL was located in both the nucleus and cytoplasm but predominantly in the nucleus. Scale bar, 3 μm.

Figure 3. Continued

(D) Oligo #4 forms a triplex structure with the BRCA1 DNA promoter. The indicated RNA oligos (to #5) were incubated with a biotin-labeled DNA promoter fragment (−1655, −1586) and the formation of DNA: RNA triplexes were monitored by EMSA. The tiled 20 nt RNA oligos (blue) are displayed above.

(E) DNA:RNA triplexes are resistant to RNase H digestion. Triplexes (lanes 2–4), formed by incubating a biotin-labeled BRCA1 DNA promoter fragment (−1685, −1566) with 68-nt wild RNA oligos (1112, 1179) (Oligo-wt), were treated with 30 U of RNase H (H) or RNase A (A) and analyzed by EMSA. Lane 5 shows DNA fragments incubated with the mutant RNA oligos (Oligo-mut).

(F) ChIRP analysis of CISAL in the regulatory regions of BRCA1(−1627, −1606) but not GAPDH. The cross-linked CAL-27 cell lysates were incubated with biotinylated DNA probes against CISAL, and the binding complexes were recovered using streptavidin-conjugated magnetic beads. qPCR was performed to detect enrichment of the specific regulatory regions associated with CISAL.

***p<0.001, one-way ANOVA followed by Dunnett's tests for multiple comparisons. Data are represented as mean ±SEM.

We therefore evaluated whether CISAL could interfere with the BRCA1 TFs at the promoter. The ENCODE project (encodeproject.org/ENCODE/) produced numerous ChIP-sequencing (ChIP-seq) datasets that map the genomic locations of TF binding in various types of tissues and cell lines. Cancer-associated TFs can be defined by combining the Entrez cancer gene list (Domazet-Loso and Tautz, 2010) with ENCODE. We screened the human ENCODE database for cancer-associated TFs that interact with BRCA1 promoter in four of commonly used cancer cell lines (GM12878, K562, HepG2, and Hela-S3) and identified dozens of TFs that are associated with the BRCA1 promoters (Figure 4A). Among these TFs, GABPA was most frequently enriched in the common region at BRCA1 promoter in five cancer cell lines and liver tissues (Figure 4B). We further performed de novo motif discovery on GABPA peaks and observed that the 5'–CTCTTCCGTC–3' (reverse complement: 5'–GACGGAAGAG–3') motif was highly enriched (Figures 4C and 4D). Interestingly, GABPA has been reported to be a critical activator of BRCA1 expression (Atlas et al., 2000). As expected, we found that GABPA knockdown reduced BRCA1 levels in CAL-27 and SCC-9 cells (Figures S9A and S9B), whereas overexpression of GABPA upregulated BRCA1 levels in both cell lines (Figure S9C). ChIP and luciferase reporter assays identified the transcriptional functionality of GABPA as well (Figures 4E–4G).

We then explored the effect of CISAL on GABPA transcriptional activity. Enforced expression of CISAL but not mut-CISAL (contains a mutant binding site in BRCA1 promoter region) reduced BRCA1 expression (Figure 4H), GABPA/RNA pol II occupancy (Figures 4I, S9D, and S9E), and transcriptional functionality of BRCA1 promoter (Figure 4J), subsequently modulating BRCA1 downstream signaling miR-593-MFF (Figures S9F and S9G). Furthermore, functional assays showed that enforced CISAL, but not mut-CISAL, increased mitochondrial fission and cisplatin sensitivity in CAL-27 and SCC-9 cells (Figure S9H). In contrast, silencing CISAL induced upregulation of GABPA/RNA pol II occupancy (Figures 4K, S9I, and S9J), transcriptional functionality of BRCA1 promoter (Figure 4L), and modification of BRCA1 downstream signaling (Figures S9K and S9L). Luciferase reporter assay further confirmed that enforced GABPA levels attenuated inhibition of BRCA1 transcriptional activity by CISAL overexpression. However, transfection of mutant CISAL-binding sites in BRCA1 promoter abolished the effect of enforced CISAL expression, wherease mutant GABPA-binding sites abrogated the effect of both CISAL and GABPA overexpression on BRCA1 transcriptional activity (Figure 4M). All together, these results show that GABPA is a key transcriptional activator in our cellular system and that CISAL inhibits BRCA1 expression through counteracting GABPA binding at the BRCA1 promoter region.

CISAL Sequesters GABPA Away from Regulatory Binding at BRCA1 Promoter

To determine the precise role of CISAL in interfering with GABPA binding, we first considered CISAL competing GABPA-binding sequence; however, no possible accessibility exists near GABPA-binding region (Figure 3A), and ChIRP assay also identified no occupancy of CSIAL in GABPA target DNA sequence (Figure S9M). We therefore decided to focus on the interaction between CISAL and GABPA, because CISAL was tethered upstream of GABPA-binding sites by DNA-RNA formation (Figure 3) where it may possibly sequester GABPA away from the regulatory region. RNA immunoprecipitation (RIP) assays revealed that CISAL could interact with endogenous GABPA in TSCC cells (Figure 5A). RNA pull-down assay also identified that CISAL could interact with recombinant GABPA and endogenous GABPA in TSCC cells (Figure 5B). To ascertain how CISAL interacted with GABPA, we used serial CISAL deletion analysis (Figures 5C and 5D) and ChIP-qPCR, which revealed that CISAL deletion to 900nt from its 5'-end preserved its ability to block GABPA binding, whereas the truncated 700nt abrogated such effect (Figure 5C). Consistently, RNA pull-down assay indicated that CISAL deletion to 900nt presented affinity with endogenous GABPA (Figure 5D). Furthermore, we engineered an allele of CISAL that can be artificially recruited to upstream binding sites of GABPA in GAL4-*BoxB*-tethering-based reporter assay (Li et al., 2013). Addition of *BoxB*

Figure 4. CISAL Represses BRCA1 Transcriptional Activity through Inhibition of GABPA Binding with BRCA1 Promoter

(A) Heatmap of selected TFs from Entrez cancer gene list in four commonly used ENCODE cell lines. Cells are sorted based on their RNA-seq data, and the color indicates whether each TF has binding peaks in the BRCA1 promoter. The TFs are hierarchically clustered using Ward's method.

(B) Distribution of GABPA occupancy frequencies in BRCA1 promoter in five different cancer cell lines and liver tissue based on ChIP-seq database. The most enriched peaks are highlighted.

(C) Motif analysis (motif-counter) showing enriched GABPA motif in BRCA1 promoter and the arrow indicates that the highest score binding sites consistently located in the forward strand, highlighted in panel B.

(D) Representation of CISAL and GABPA binding elements in BRCA1 promoter.

(E) ChIP-qPCR analysis of the GABPA genomic occupancy in the BRCA1 promoter in CAL-27 and SCC-9 cells as indicated. Immunoprecipitated DNA was measured by real-time PCR with primers to amplify the BRCA1 promoter region, including the distal site, or the GAPDH locus as a negative control region.

(F) Luciferase reporter assay demonstrating that GABPA activated BRCA1 promoter activity. CAL-27 cells with stable expression of pGL4.20 empty vector (Vector) and wild-type (wt-GABPA BS) or mutant (mut-GABPA BS) BRCA1-promoter-delivered pGL4.20 vectors were transiently co-transfected with GABPA expressing plasmids and pRL-TK.

(G) Luciferase assay demonstrating that GABPA knockdown inhibits BRCA1 promoter activity in CAL-27 cells.

(H–J) Overexpression of wild-type CISAL but not the mutant CISAL (mut-CISAL) represses BRCA1 expression (H), GABPA occupancy in BRCA1 promoter (I) and BRCA1 transcriptional activity (J) in CAL-27 cells.

(K and L) Knockdown of CISAL increases GABPA occupancy at BRCA1 promoter (K) and BRCA1 promoter activity (L) in CAL-27 cells.

(M) Luciferase assay demonstrating that GABPA overexpression attenuates the inhibition of BRCA1 promoter activity, by enhancing expression of CISAL but not mut-CISAL in CAL-27 cells stably transfected with wild-type BRCA1 promoter, whereas overexpression of CISAL demonstrated no effect on BRCA1 promoter activity when transfected with mutant CISAL-binding sites (mut-CISAL BS), and the luciferase signals were similar in groups transfected with mutant GABPA binding sites (mut-GABPA BS).

***$p < 0.001$ by 2-tailed Student's t test (E) or 1-way ANOVA followed by Dunnett's tests for multiple comparisons (F–M). Data are represented as mean ±SEM.

RNA element to CISAL (*BoxB*-CISAL) allowed the fusion transcript to be recruited by the RNA-binding domain of λN protein fused with the GAL4 DNA-binding domain (λN–GAL4) when CISAL-binding sequence was deleted and substituted with 5xUAS sites (Figure 5E). We confirmed that GAL4 could be tethered at 5xUAS region and *BoxB*-CISAL co-immunoprecipitated by GAL4 (Figure 5E). Luciferase assay indicated recruitment of CISAL at 5xUAS site, significantly repressing transcription, but enforced overexpression of GABPA attenuated the inhibition if the promoter included wild GABPA-binding sites. However, the mutant GABPA sequence abolished the effect of both *BoxB*-CISAL and GABPA on transcriptional activity (Figure 5F). These data suggest that CISAL is specifically tethered upstream of GABPA-targeted DNA sequence, subsequently sequestering GABPA away from its regulatory binding sites at BRCA1 promoter and inhibiting BRCA1 transcription.

Next, we confirmed the role of truncated CISAL in modulating BRCA1 signaling pathway, mitochondrial fission, and cisplatin sensitivity in TSCC cells. CISAL (1-700) was unable to inhibit BRCA1 expression (Figure S10A) and transcriptional activity (Figures 5G, S10B, and S10C), or BRCA1 downstream signaling (Figure S10D, E), consequently losing the ability to boost mitochondrial fission and cisplatin sensitivity (Figure S10F). In contrast, overexpression of truncated CISAL (1-900) in CISAL-silenced cancer cells restored the function of CISAL related to BRCA1 levels (Figure S10G), GABPA/RNA pol II occupancy (Figures 5H, S10H, and S10I), BRCA1 transcriptional activity (Figure 5I), expression of downstream genes (Figures S10J and S10K), as well as mitochondrial fission and cisplatin sensitivity (Figure S10L).

CISAL Regulates Cisplatin Chemosensitivity in TSCC *In Vivo*

To further validate the relationship between CISAL and BRCA1 in the regulation of cisplatin sensitivity, we established TSCC xenografts *in vivo*. CISAL knockdown led to a significant increase in CAL-27 tumor growth in the presence of cisplatin (Figures 6A–6C). CISAL expression was downregulated in the CISAL silencing group, whereas BRCA1 expression was increased (Figures 6D and S11A–S11C). We also analyzed BRCA1 downstream genes (Fan et al., 2015b) and found that the expression of miR-593 was increased in tumors with CISAL knockdown, whereas MFF expression was decreased (Figures S11C andS11D). Apoptosis was also attenuated upon CISAL knockdown under cisplatin treatment (Figures 6E and S11E). On the other hand, PCNA expression was not found to be significantly different in each group (Figure S11C), indicating that the influence of CISAL was not secondary to impaired proliferation. In contrast, overexpression of CISAL inhibited tumor growth and enhanced cisplatin sensitivity (Figures 6F–6H), whereas apoptotic tumor cells, CISAL, BRCA1, miR-593-5p, and MFF expression (Figures 6I and S12A–S12E), were also detected, supporting the idea that enforced CISAL expression inhibits BRCA1 transcription *in vivo*. These results suggest that CISAL regulates cisplatin sensitivity and apoptosis in TSCC cells by directly modulating BRCA1 transcription *in vivo*.
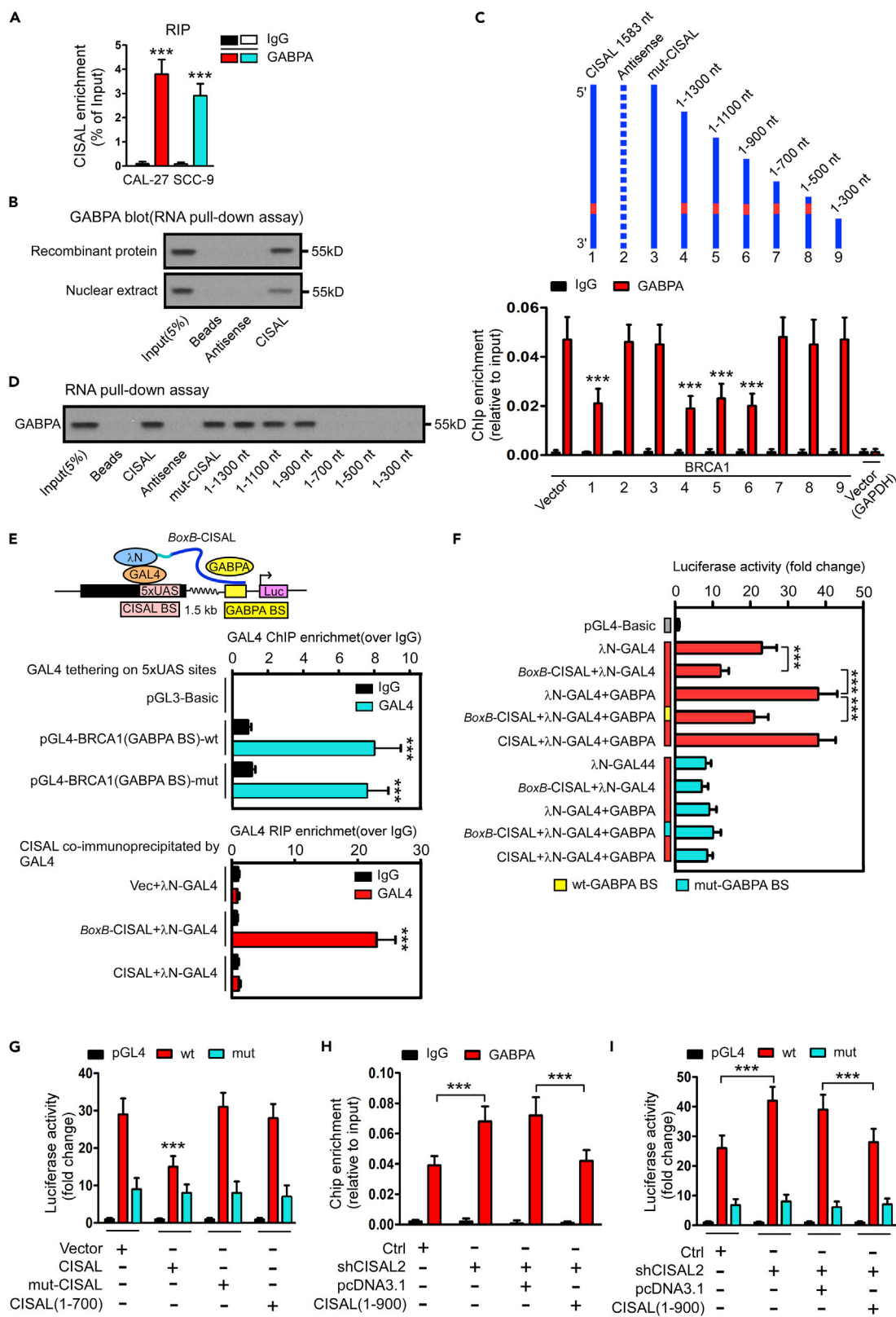
Figure 5. CISAL Sequesters GABPA away from Regulatory Binding Sites at BRCA1 Promoter

(A) RT-qPCR analysis of CISAL enrichment by GABPA in the RIP assay in CAL-27 and SCC-9 cells. Normal IgG was used as a nonspecific control.

(B) Western blot analysis showing that CISAL associates with GABPA, as indicated by the pull-down assay with *in vitro* translated GABP or nuclear extracts of CAL-27 cells. Antisense CISAL was used as a negative control RNA in the pull-down assay.

(C and D) Serial deletions of CISAL were used in ChIP-qPCR analysis (C) and RNA pull-down assays (D) to identify valid length of CISAL, required for physical interaction with GABPA and for sequestering GABPA away from the its downstream binding sites at BRCA1 promoter in CAL-27 cells. Immunoprecipitated DNA was measured by real-time PCR with primers to amplify the BRCA1 promoter region, including the GAPDH locus as a negative control.

(E) Schematic diagram of the *x*-tethering system on CISAL, which is upstream of GABPA binding sites in BRCA1 promoter-linked luciferase (Luc). CISAL-binding sequence was substituted with 5xUAS and a chimeric RNA by fusing CISAL to *BoxB* viral RNA *BoxB*-CISAL. N-GAL4 fusion protein tethers *BoxB*-CISAL to the 5xUAS sites. Middle panel indicate efficiency of GAL4 tethering at 5xUAS region by ChIP-qPCR analysis. Lower panel shows that BoxB-CISAL instead of CISAL co-immunoprecipitated by GAL4.

(F) Luciferase assay shows *BoxB*-CISAL repressed BRCA1 promoter activity, which was rescued upon enhancement of GABPA expression in CAL-27 cells with wild GABPA-binding sites transfection and using mutant GABPA-binding sites as a negative control.

(G) Site-directed mutagenesis of 1–700 nt of CISAL leads to a loss of the effect on BRCA1 promoter activity in CAL-27 cells.

(H and I) Forced expression of the truncated CISAL (1–900) abolished the increase of GABPA occupancy (H) and BRCA1 transcriptional activity (I) by silencing endogenous CISAL in CAL-27 cells.

***p< 0.001 by 2-tailed Student's t test (A, C, E, and G–I) or 1-way ANOVA followed by Dunnett's tests for multiple comparisons (F). Data are represented as mean ±SEM.

High CISAL and Low BRCA1 Expression Are Associated with Favorable Neoadjuvant Chemosensitivity and Prognosis of TSCC Patients

To evaluate the clinical relevance of CISAL and BRCA1 expression, we performed a retrospective analysis of TSCC samples (TSCCs) from 113 patients treated with platinum-based neoadjuvant chemotherapies. *In situ* hybridization (ISH) and immunohistochemical staining demonstrated that CISAL expression was higher, whereas BRCA1 expression was lower in chemosensitive TSCCs, as compared with resistant tumors (Figure 7A). A significant difference in the expression profile of chemosensitive and chemoresistant TSCCs were determined by the percentage of positive cells (Figure 7B). Consequently, cisplatin-sensitive TSCCs exhibited a higher percentage of apoptotic cells (Figure 7A). Additionally, a Spearman order correlation analysis showed that CISAL levels were reversely correlated with those of BRCA1 in TSCCs (rs = −0.733, p<0.001) (Figure 7C). Notably, TCGA analysis also found an inverse correlation in CISAL and BRCA1 expression in bladder carcinoma (Figure S13).

Next, we analyzed the association of CISAL and BRCA1 expression with the clinicopathological status of TSCC patients (Table S3). No significant correlation was observed between CISAL or BRCA1 expression and sex, age, lymph node status, or clinical stage. However, CISAL and BRCA1 expression were significantly associated with cisplatin sensitivity. Moreover, we evaluated the correlation between CISAL and BRCA1 expression and patient overall survival (OS). The cumulative survival rate at 60 months was 43.28% and 43.66% in patients with high CISAL and low BRCA1 expression, respectively; however, the corresponding rate was only 21.74% and 19.05% in those with low CISAL and high BRCA1 expression, respectively (Table S3). A univariate Cox regression analysis indicated that TSCC patients with high CISAL expression level or low BRCA1 levels had longer OS (Table 1 and Figure 7D). Furthermore, a multivariate Cox regression analysis revealed that high CISAL expression and low BRCA1 expression are independent prognostic factors for better OS in patients with TSCC (Table 1). All together, our data suggest that CISAL and its direct target BRCA1 correlate with neoadjuvant chemosensitivity and patient OS with TSCC, whereas CISAL play an important role as DNA binding cofactor by directly interacting with TF, rather than competing in binding with TF or the decoy mechanism (Figure 7E).

DISCUSSION

In this study, we show that the lncRNA CISAL regulates mitochondrial fission and cisplatin sensitivity through BRCA1 signaling. In exploring the mechanism by which BRCA1 transcription is inhibited, we found that CISAL can be specifically tethered at BRCA1 promoter by formation of an RNA–DNA triplex structure, which subsequently sequesters BRCA1 TF-GABPA away from its binding to regulatory DNA target. Importantly, we show that CISAL-BRCA1 expression is associated with patients' survival in multiple types of human cancer and TSCC patients' neoadjuvant chemosensitivity. These results provide mechanistic and translational insights into neoadjuvant chemosensitivity and suggest that targeting CISAL-BRCA1 signaling pathway could be used for predicting or improving neoadjuvant chemosensitivity.
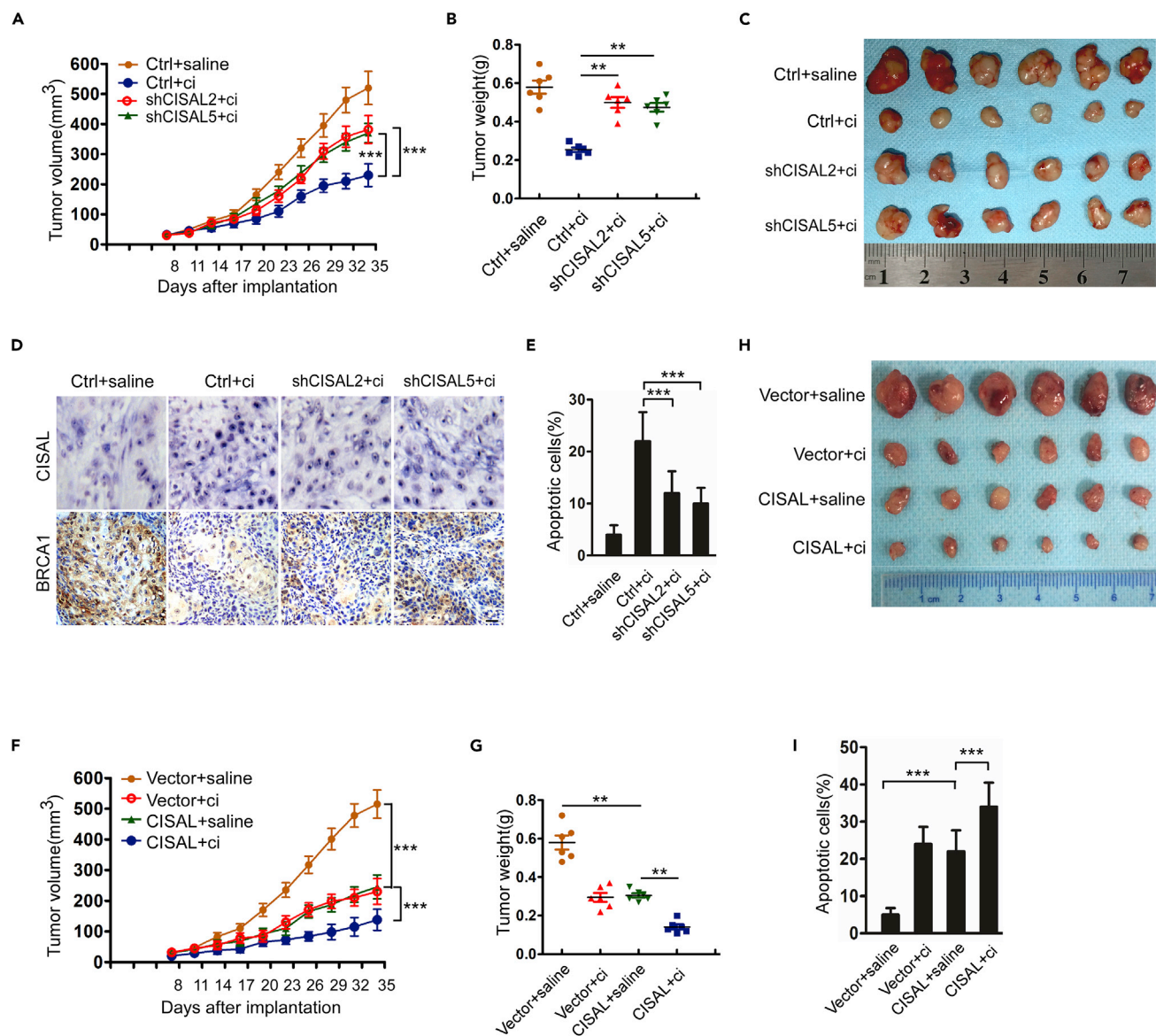
Figure 6. CISAL Regulates Apoptosis and Cisplatin Sensitivity in CAL-27 Cell Xenografts *In Vivo*

(A) BALB/c nude mice bearing xenografts of CAL-27 cells with stable knockdown of CISAL or negative controls (Ctrl) were treated with saline or cisplatin (n = 6 per group) and tumor growth was monitored. Results are expressed as the mean ± SEM.

(B) Tumor weight for each group.

(C) Photomicrographs of tumors from each group at day 35.

(D) CISAL knockdown decreases CISAL expression but upregulates BRCA1 expression in CAL-27 cell xenografts upon treatment with cisplatin. CISAL and BRCA1 expression was detected by ISH and IHC, respectively in tissues from different treated groups.

(E) TUNEL assays showed that apoptosis in response to cisplatin was attenuated by CISAL knockdown.

(F–I) BALB/c nude mice bearing xenografts of CAL-27 cells with stable CISAL expression or control vector were treated with saline or cisplatin (n = 6 per group) and tumor was monitored over time (F); tumor weight (G) for each group, photomicrographs of tumors (H), and apoptotic dells (I) from each group at day 35.

***p< 0.001, 2-way ANOVA followed by Bonferroni's post-test (A and F); **p<0.01 and ***p<0.001, 1-way ANOVA followed by Dunnett's tests for multiple comparisons (B, E, G, and I); scale bar, 20 μm. Data are represented as mean ±SEM.

Numerous studies strongly suggest that lncRNAs in "gene desert" regions play significant roles in tumor occurrence and development and could be used as a biomarker (Bonasio and Shiekhattar, 2014; Vance and Ponting, 2014). LncRNAs were initially described as regulators of chromatin organization and gene expression (Engreitz et al., 2013; Giovarelli et al., 2014). LncRNAs can interface with the genome at the
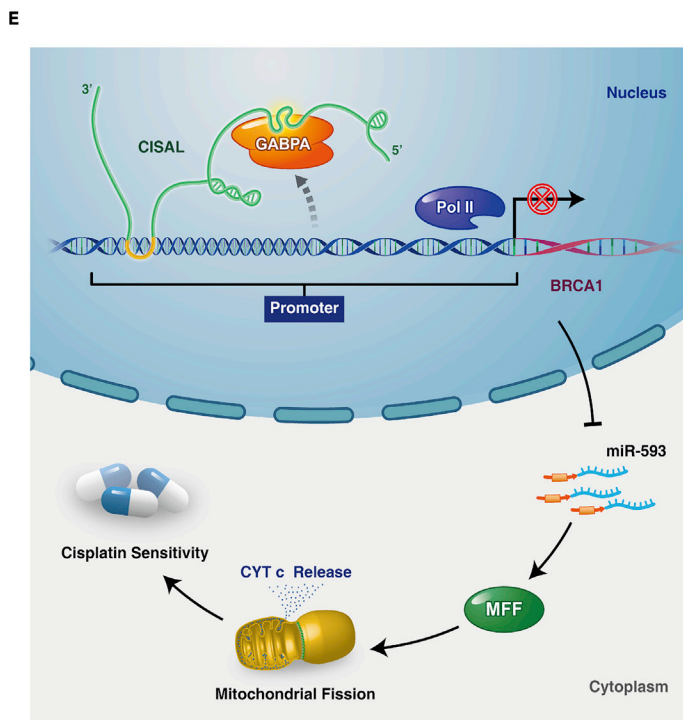
A

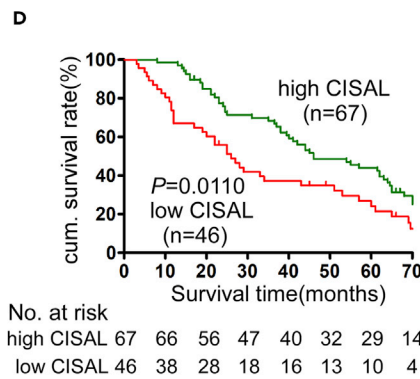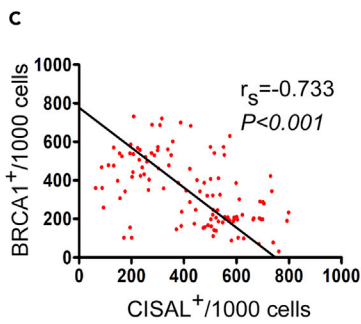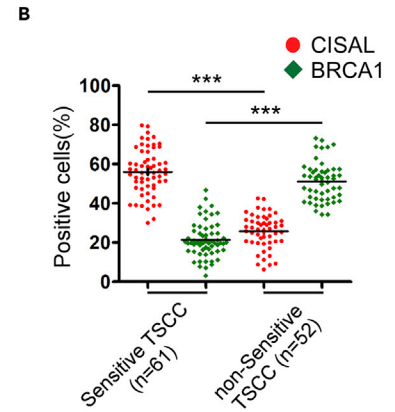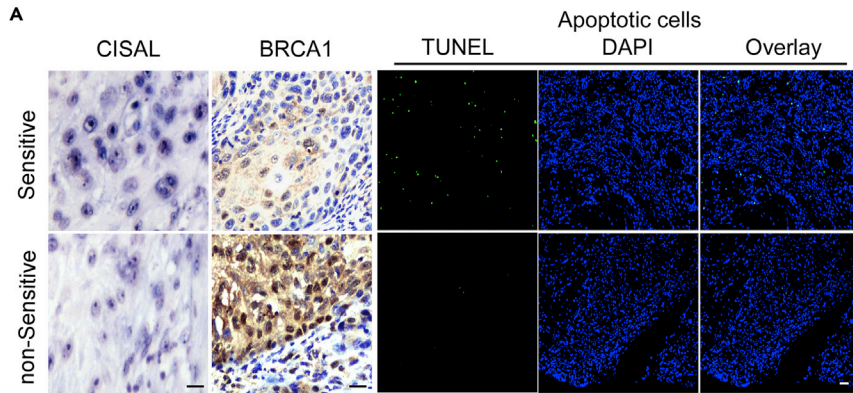**B**

C

D

E

Figure 7. High CISAL and Low BRCA1 Expression Correlates with Favorable Neoadjuvant Chemosensitivity and Prognosis in TSCC Patients

(A) CISAL and BRCA1 expression and apoptosis were compared in chemosensitive and nonsensitive TSCC tumor samples. CISAL and BRCA1 expression was analyzed by ISH and IHC (×200), respectively; apoptosis was detected using TUNEL assays; scale bar, 20 μm.

(B) Quantification of CISAL and BRCA1 expression in chemosensitive and nonsensitive TSCC tumors; ***p<0.001, 2-tailed Student's t test.

(C) Associations of CISAL and BRCA1 expression in TSCC analyzed by Spearman rank order correlation.

(D) Kaplan-Meier survival curves for TSCC patients were plotted for CISAL and BRCA1 expression, and survival differences were analyzed using a logrank test.

(E) Schematic representation of our proposed model of direct interaction of CISAL with BRCA1 promoter to sequester the downstream GABPA away from transcriptional regulatory binding sites, silencing BRCA1 transcription, subsequently upregulating mitochondrial fission and cisplatin sensitivity in carcinoma cells.

sequence level and fold into tertiary structures capable of specific interactions with proteins; therefore, they can regulate gene expression at different levels. In fact, several studies have uncovered many specific examples and general classes of lncRNAs that repress or activate transcription (Bonasio and Shiekhattar, 2014). Indeed, the direct interaction of lncRNAs and TFs to inhibit transcription activities is rarely reported (Long et al., 2017).

In an effort to understand how lncRNAs target the genome, computational approaches are being used to predict the interaction of lncRNAs and chromatin or DNA by (1) suggesting candidate lncRNA-associated TFs according to the enrichments of their binding motifs; (2) proposing the involvement of lncRNA in transcriptional enhancement or repression from enrichments of relevant chromatin markers; and (3) identifying near-complementary DNA sequences within lncRNA-associated regions that might indicate direct RNA–DNA triplex formation (Buske et al., 2012; Vance et al., 2014). Indeed, we first calculated the binding potential and found a complementary sequence between the CISAL and BRCA1 promoter before further experimental validation. The genomic associations observed between lncRNAs and chromatin could be accomplished through direct base pairing between RNA and DNA sequences to form RNA-DNA triplexes, possibly through Hoogsteen base pairing (Mondal et al., 2015). Based on the bioinformatics analysis and rigorously controlled experiments, we identified that CISAL formed RNA–DNA triplex with BRCA1 promoter.

Understandably, nuclear lncRNAs mainly regulate transcription activity through histone modification or direct/indirect interaction with TFs. We observed no association between CISAL and histone modification; however, we found a direct interaction between CISAL and GABPA. Broadly, lncRNAs exercise many roles including recruiters, decoys, stimuli, scaffolds, or some combinations thereof (Long et al., 2017). For the repression of transcription, lncRNA could plausibly act as a"sponge" or "decoy," binding and activating TF and preventing it from interacting with its DNA/RNA target by binding functionally and inactivating the protein (Kino et al., 2010). LncRNAs may also compete with TFs for DNA-binding sites (Pfingsten et al., 2012) or by determining cocrystal structures of the protein-DNA and protein-lncRNA complexes (Hudson and Ortlund, 2014). Interestingly, we found that only the tethered CISAL at BRCA1 promoter sequestered GABPA away from binding to BRCA1 promoter, because mut-CISAL lost its binding affinity to BRCA1 promoter, thereby disabling transcription repression and even reserving the interaction with GABPA. Therefore, our study proposes a model where lncRNAs specifically regulate gene transcription through tethering lncRNAs at promoter region by RNA–DNA triplex, directly interacting with TF. However, we cannot rule out the possibility that some of the DNA/RNA binding elements are indirectly involved in this procedure.

Emerging data suggest that abnormal mitochondrial morphology may be relevant to various aspects of disease and apoptosis (Trotta and Chipuk, 2017). We have also first revealed the important role of mitochondrial fission in cisplatin sensitivity (Fan et al., 2015a, 2015b). Until now, whether lncRNA is involved in the regulation of cisplatin chemosensitivity through mitochondrial dynamics remains unclear. Our present work indicates that CISAL can regulate mitochondrial fission and cisplatin chemosensitivity through a BRCA1-dependent signaling axis. This work sheds new light to the understanding of mitochondrial fission and chemosensitivity. BRCA1 also plays a pivotal role in DNA repair (Suberbielle et al., 2015). Whether the CISAL/BRCA1 axis mediates the DNA repair pathway requires further investigation. Importantly, our study provides mechanistic and translational insights of CISAL in neoadjuvant chemosensitivity. Regarding the prediction of chemosensitivity, the basal expression of CISAL and the induction of CISAL expression by neoadjuvant chemotherapy had to be detected. Our data demonstrate that higher expression of CISAL was associated with neoadjuvant chemosensitivity. CISAL-BRCA1 axis is not only associated with TSCC patients' neoadjuvant chemosensitivity and OS but is also correlated with OS in multiple types of human cancer, based on TCGA analysis, providing a base for future studies to evaluate the role of CISAL in other types of cancers.

Variable	Cases Number	HR (95% CI)	P
Univariate Analysis			
Sex Male vs female	62/51	1.107(0.604–2.030)	0.604
Age(years) <50 vs ≥50	37/76	1.186(0.739–1.904)	0.593
Node metastasis N0 vs N+	47/66	1.579(1.169–2.132)	0.023
Clinical stage III VS IV	70/43	2.040(1.368–3.041)	<0.001
Cisplatin Sensitive vs non-sensitive	61/52	0.708(0.509–0.986)	0.046
CISAL Low vs high	46/67	1.687(1.207–2.357)	0.011
BRCA1 Low vs high	71/42	1.716(1.207–2.439)	0.009
Multivariate Analysis			
Node metastasis N0 vs N+	47/66	1.686(1.328–2.140)	0.014
Clinical stage III VS IV	70/43	2.119(1.374–3.269)	<0.001
Cisplatin Sensitive vs non-sensitive	61/52	0.667(0.496–0.896)	0.032
CISAL Low vs high	46/67	1.820(1.306–2.537)	0.002
BRCA1 Low vs high	71/42	1.862(1.269–2.731)	<0.001

Table 1. Univariate and Multivariate Analysis of Factors Associated with Overall Survival of Patients with TSCC

In summary, we are beginning to achieve a full understanding of the molecular mechanism responsible for lncRNA-mediated regulation of transcription. Our study proposes a model where the lncRNA CISAL regulates TSCC mitochondrial fission and cisplatin-based neoadjuvant chemosensitivity, by tethering at BRCA1 promoter and sequestering downstream BRCA1 TF-GABPA away from regulatory binding region, thereby inhibiting BRCA1 transcription and its downstream signaling pathway. Moreover, TCGA analysis revealed that CISAL-BRCA1 axis is associated with OS in multiple types of cancers, suggesting that CISAL-BRCA1 axis could be used as a target to predict or improve neoadjuvant chemosensitivity and patients' overall survival.

Limitations of the Study

In this study, we demonstrated that CISAL directly binds the BRCA1 promoter and forms an RNA-DNA triplex structure, sequestering BRCA1 transcription factor, GABPA, away from the downstream regulatory binding region, rather than current functionality of lncRNAs in transcriptional regulatory programs, such as competing the binding sites or playing as the decoy/sponge. It is plausible that CISAL plays important roles in 3D chromatin structure formation. Although the short-range chromatin interactions around 2kb cannot be detected by current technology, future studies evaluating CISAL and long-range interactions between the BRCA1 promoter and its enhancers would likely yield deeper mechanistic insight into the regulation of CISAL-BRCA1 signaling pathway. In addition, taking into consideration the CISAL distribution throughout the nucleoplasm and cytoplasm, further studies are needed to identify additional binding partners and functional properties of CISAL.

METHODS

All methods can be found in the accompanying Transparent Methods supplemental file.

SUPPLEMENTAL INFORMATION

Supplemental Information can be found online at https://doi.org/10.1016/j.isci.2020.100835.

AUTHOR CONTRIBUTIONS

S.Fan, J.S.L., and Y.R. designed the study. S.Fan, T.T, X.B.L., and X.Y.L. designed the experiments. S.Fan, T.T., X.B.L., X.Y.L., Z.H.Y, S.R.L., and Z.Y.L. performed the experiments and the statistical analysis of the results with the assistance from X.F.L., F.Y.L., G.K.P., S.L.X., Y.Z., X.Y.L., Z.P.O., W.X.C.,B.W.L., Y.P., L.P.X., Z.L.Z., S.S., H.Q.Z., S.G.L., M.L., Q.X.L., B.H.Z., Z.M.T., L.L.H., F.K., and D.C.L., B.A.T. and S.F. provided reagents and helped with the experiments. J.S.L. and Y.R. reviewed the data with special emphasis on the clinical aspects. S.Fan, J.S.L., and B.A.T. wrote the manuscript.

DECLARATION OF INTERESTS

The authors declare no competing interests.

REFERENCES

Atlas, E., Stramwasser, M., Whiskin, K., and Mueller, C.R. (2000). GA-binding protein alpha/beta is a critical regulator of the BRCA1 promoter. Oncogene 19, 1933–1940.

Bian, Z., Zhang, J., Li, M., Feng, Y., Wang, X., Zhang, J., Yao, S., Jin, G., Du, J., Han, W., et al. (2018). LncRNA-FEZF1-AS1 promotes tumor proliferation and metastasis in colorectal cancer by regulating pkm2 signaling. Clin. Cancer Res. 24, 4808–4819.

Bonasio, R., and Shiekhattar, R. (2014). Regulation of transcription by long noncoding RNAs. Annu. Rev. Genet. 48, 433–455.

Buske, F.A., Bauer, D.C., Mattick, J.S., and Bailey, T.L. (2012). Triplexator: detecting nucleic acid triple helices in genomic and transcriptomic data. Genome Res. 22, 1372–1381.

Cabili, M.N., Trapnell, C., Goff, L., Koziol, M., Tazon-Vega, B., Regev, A., and Rinn, J.L. (2011). Integrative annotation of human large intergenic noncoding RNAs reveals global properties and specific subclasses. Genes Dev. 25, 1915–1927.

Carpenter, S., Aiello, D., Atianand, M.K., Ricci, E.P., Gandhi, P., Hall, L.L., Byron, M., Monks, B., Henry-Bezy, M., Lawrence, J.B., et al. (2013). A long noncoding RNA mediates both activation and repression of immune response genes. Science 341, 789–792.

Derrien, T., Johnson, R., Bussotti, G., Tanzer, A., Djebali, S., Tilgner, H., Guernec, G., Martin, D., Merkel, A., Knowles, D.G., et al. (2012). The GENCODE v7catalog of human long noncoding RNAs: analysis of their gene structure, evolution, and expression. Genome Res. 22, 1775–1789.

Domazet-Loso, T., and Tautz, D. (2010). Phylostratigraphic tracking of cancer genes suggests a link to the emergence of multicellularity in metazoa. BMC Biol. 8, 66.

Engreitz, J.M., Pandya-Jones, A., McDonel, P., Shishkin, A., Sirokman, K., Surka, C., Kadri, S., Xing, J., Goren, A., Lander, E.S., et al. (2013). The Xist lncRNA exploits three-dimensional genome architecture to spread across the X chromosome. Science 341, 1237973.

Fan, S., Chen, W.X., Lv, X.B., Tang, Q.L., Sun, L.J., Liu, B.D., Zhong, J.L., Lin, Z.Y., Wang, Y.Y., Li, Q.X., et al. (2015a). miR-483-5p determines mitochondrial fission and cisplatin sensitivity in tongue squamous cell carcinoma by targeting FIS1. Cancer Lett. 362, 183–191.

Fan, S., Liu, B., Sun, L., Lv, X.B., Lin, Z., Chen, W., Chen, W., Tang, Q., Wang, Y., Su, Y., et al. (2015b). Mitochondrial fission determines cisplatin sensitivity in tongue squamous cell carcinoma through the BRCA1-miR-593-5p-MFF axis. Oncotarget 6, 14885–14904.

Gibson, M.K., Li, Y., Murphy, B., Hussain, M.H., DeConti, R.C., Ensley, J., Forastiere, A.A., and Eastern Cooperative Oncology, G. (2005). Randomized phase III evaluation of cisplatin plus fluorouracil versus cisplatin plus paclitaxel in advanced head and neck cancer (E1395): an

intergroup trial of the Eastern Cooperative Oncology Group. J. Clin. Oncol. 23, 3562–3567.

Giovarelli, M., Bucci, G., Ramos, A., Bordo, D., Wilusz, C.J., Chen, C.Y., Puppo, M., Briata, P., and Gherzi, R. (2014). H19 long noncoding RNA controls the mRNA decay promoting function of KSRP. Proc. Natl. Acad. Sci. U S A 111, E5023–E5028.

Greco, C.M., and Condorelli, G. (2015). Epigenetic modifications and noncoding RNAs in cardiac hypertrophy and failure. Nat. Rev. Cardiol. 12, 488–497.

Hacisuleyman, E., Goff, L.A., Trapnell, C., Williams, A., Henao-Mejia, J., Sun, L., McClanahan, P., Hendrickson, D.G., Sauvageau, M., Kelley, D.R., et al. (2014). Topological organization of multichromosomal regions by the long intergenic noncoding RNA Firre. Nat. Struct. Mol. Biol. 21, 198–206.

Hah, N., Murakami, S., Nagari, A., Danko, C.G., and Kraus, W.L. (2013). Enhancer transcripts mark active estrogen receptor binding sites. Genome Res. 23, 1210–1223.

Herriges, M.J., Swarr, D.T., Morley, M.P., Rathi, K.S., Peng, T., Stewart, K.M., and Morrisey, E.E. (2014). Long noncoding RNAs are spatially correlated with transcription factors and regulate lung development. Genes Dev. 28, 1363–1379.

Heward, J.A., and Lindsay, M.A. (2014). Long non-coding RNAs in the regulation of the immune response. Trends Immunol. 35, 408–419.

Hu, J., Lieb, J.D., Sancar, A., and Adar, S. (2016). Cisplatin DNA damage and repair maps of the human genome at single-nucleotide resolution. Proc. Natl. Acad. Sci. U S A 113, 11507–11512.

Hu, X., Feng, Y., Zhang, D., Zhao, S.D., Hu, Z., Greshock, J., Zhang, Y., Yang, L., Zhong, X., Wang, L.P., et al. (2014). A functional genomic approach identifies FAL1 as an oncogenic long noncoding RNA that associates with BMI1 and represses p21 expression in cancer. Cancer Cell 26, 344–357.

Hudson, W.H., and Ortlund, E.A. (2014). The structure, function and evolution of proteins that bind DNA and RNA. Nat. Rev. Mol. Cell Biol. 15, 749–760.

Kim, S.W., Fishilevich, E., Arango-Argoty, G., Lin, Y., Liu, G., Li, Z., Monaghan, A.P., Nichols, M., and John, B. (2015). Genome-wide transcript profiling reveals novel breast cancer-associated intronic sense RNAs. PLoS One 10, e0120296.

Kino, T., Hurt, D.E., Ichijo, T., Nader, N., and Chrousos, G.P. (2010). Noncoding RNA gas5 is a growth arrest- and starvation-associated repressor of the glucocorticoid receptor. Sci. Signal. 3, ra8.

Lam, M.T., Cho, H., Lesch, H.P., Gosselin, D., Heinz, S., Tanaka-Oishi, Y., Benner, C., Kaikkonen, M.U., Kim, A.S., Kosaka, M., et al. (2013). Rev-Erbs repress macrophage gene expression by inhibiting enhancer-directed transcription. Nature 498, 511–515.

Li, W., Notani, D., Ma, Q., Tanasa, B., Nunez, E., Chen, A.Y., Merkurjev, D., Zhang, J., Ohgi, K., Song, X., et al. (2013). Functional roles of enhancer RNAs for oestrogen-dependent transcriptional activation. Nature 498, 516–520.

Liu, H.T., Liu, S., Liu, L., Ma, R.R., and Gao, P. (2018). EGR1-mediated transcription of lncRNA-HNF1A-AS1 promotes cell-cycle progression in gastric cancer. Cancer Res. 78, 5877–5890.

Liu, X., Xiao, Z.D., Han, L., Zhang, J., Lee, S.W., Wang, W., Lee, H., Zhuang, L., Chen, J., Lin, H.K., et al. (2016). LncRNA NBR2 engages a metabolic checkpoint by regulating AMPK under energy stress. Nat. Cell Biol. 18, 431–442.

Long, Y., Wang, X., Youmans, D.T., and Cech, T.R. (2017). How do lncRNAs regulate transcription? Sci. Adv. 3, eaao2110.

Melo, C.A., Drost, J., Wijchers, P.J., van de Werken, H., de Wit, E., Oude Vrielink, J.A., Elkon, R., Melo, S.A., Leveille, N., Kalluri, R., et al. (2013). eRNAs are required for p53-dependent enhancer activity and gene transcription. Mol. Cell 49, 524–535.

Mondal, T., Subhash, S., Vaid, R., Enroth, S., Uday, S., Reinius, B., Mitra, S., Mohammed, A., James, A.R., Hoberg, E., et al. (2015). MEG3 long noncoding RNA regulates the TGF-beta pathway genes through formation of RNA-DNA triplex structures. Nat. Commun. 6, 7743.

Peng, W.X., Koirala, P., and Mo, Y.Y. (2017). LncRNA-mediated regulation of cell signaling in cancer. Oncogene 36, 5661–5667.

Pfingsten, J.S., Goodrich, K.J., Taabazuing, C., Ouenzar, F., Chartrand, P., and Cech, T.R. (2012). Mutually exclusive binding of telomerase RNA and DNA by Ku alters telomerase recruitment model. Cell 148, 922–932.

Rapicavoli, N.A., Poth, E.M., Zhu, H., and Blackshaw, S. (2011). The long noncoding RNA Six3OS acts in trans to regulate retinal development by modulating Six3 activity. Neural Dev. 6, 32.

Rinn, J.L., Kertesz, M., Wang, J.K., Squazzo, S.L., Xu, X., Brugmann, S.A., Goodnough, L.H., Helms, J.A., Farnham, P.J., Segal, E., et al. (2007). Functional demarcation of active and silent chromatin domains in human HOX loci by noncoding RNAs. Cell 129, 1311–1323.

Russell, M.R., Penikis, A., Oldridge, D.A., Alvarez-Dominguez, J.R., McDaniel, L., Diamond, M., Padovan, O., Raman, P., Li, Y., Wei, J.S., et al. (2015). CASC15-S is a tumor suppressor lncRNA at the 6p22 neuroblastoma susceptibility locus. Cancer Res. 75, 3155–3166.

Schrock, M.S., Batar, B., Lee, J., Druck, T., Ferguson, B., Cho, J.H., Akakpo, K., Hagrass, H., Heerema, N.A., Xia, F., et al. (2017). Wwox-Brca1 interaction: role in DNA repair pathway choice. Oncogene 36, 2215–2227.

Suberbielle, E., Djukic, B., Evans, M., Kim, D.H., Taneja, P., Wang, X., Finucane, M., Knox, J., Ho, K., Devidze, N., et al. (2015). DNA repair factor BRCA1 depletion occurs in Alzheimer brains and impairs cognitive function in mice. Nat. Commun. 6, 8897.

Subramanian, A., Tamayo, P., Mootha, V.K., Mukherjee, S., Ebert, B.L., Gillette, M.A., Paulovich, A., Pomeroy, S.L., Golub, T.R., Lander, E.S., et al. (2005). Gene set enrichment analysis: a knowledge-based approach for interpreting genome-wide expression profiles. Proc. Natl. Acad. Sci. U S A 102, 15545–15550.

Suen, D.F., Norris, K.L., and Youle, R.J. (2008). Mitochondrial dynamics and apoptosis. Genes Dev. 22, 1577–1590.

Sun, S., Del Rosario, B.C., Szanto, A., Ogawa, Y., Jeon, Y., and Lee, J.T. (2013). Jpx RNA activates Xist by evicting CTCF. Cell 153, 1537–1551.

Trotta, A.P., and Chipuk, J.E. (2017). Mitochondrial dynamics as regulators of cancer biology. Cell Mol. Life Sci. 74, 1999–2017.

Ulitsky, I., and Bartel, D.P. (2013). lincRNAs: genomics, evolution, and mechanisms. Cell 154, 26–46.

Vance, K.W., and Ponting, C.P. (2014). Transcriptional regulatory functions of nuclear long noncoding RNAs. Trends Genet. 30, 348–355.

Vance, K.W., Sansom, S.N., Lee, S., Chalei, V., Kong, L., Cooper, S.E., Oliver, P.L., and Ponting, C.P. (2014). The long non-coding RNA Paupar regulates the expression of both local and distal genes. EMBO J. 33, 296–311.

Wang, J.X., Jiao, J.Q., Li, Q., Long, B., Wang, K., Liu, J.P., Li, Y.R., and Li, P.F. (2011). miR-499 regulates mitochondrial dynamics by targeting calcineurin and dynamin-related protein-1. Nat. Med. 17, 71–78.

Wang, S., Liang, K., Hu, Q., Li, P., Song, J., Yang, Y., Yao, J., Mangala, L.S., Li, C., Yang, W., et al. (2017). JAK2-binding long noncoding RNA promotes breast cancer brain metastasis. J. Clin. Invest. 127, 4498–4515.

Xing, Z., Zhang, Y., Liang, K., Yan, L., Xiang, Y., Li, C., Hu, Q., Jin, F., Putluri, V., Putluri, N., et al. (2018). Expression of long noncoding RNA YIYA promotes glycolysis in breast cancer. Cancer Res. 78, 4524–4532.

Zhong, L.P., Zhang, C.P., Ren, G.X., Guo, W., William, W.N., Jr., Sun, J., Zhu, H.G., Tu, W.Y., Li, J., Cai, Y.L., et al. (2013). Randomized phase III trial of induction chemotherapy with docetaxel, cisplatin, and fluorouracil followed by surgery versus up-front surgery in locally advanced resectable oral squamous cell carcinoma. J. Clin. Oncol. 31, 744–751.

Supplemental Information

lncRNA CISAL Inhibits BRCA1

Transcription by Forming

a Tertiary Structure at Its Promoter

Song Fan, Tian Tian, Xiaobin Lv, Xinyuan Lei, Zhaohui Yang, Mo Liu, Faya Liang, Shunrong Li, Xiaofeng Lin, Zhaoyu Lin, Shule Xie, Bowen Li, Weixiong Chen, Guokai Pan, Xinyu Lin, Zhanpeng Ou, Yin Zhang, Yu Peng, Liping Xiao, Lizao Zhang, Sheng Sun, Hanqing Zhang, Sigeng Lin, Qunxing Li, Binghui Zeng, Filippos Kontos, Yi Ruan, Soldano Ferrone, Dechen Lin, Bakhos A. Tannous, and Jinsong Li
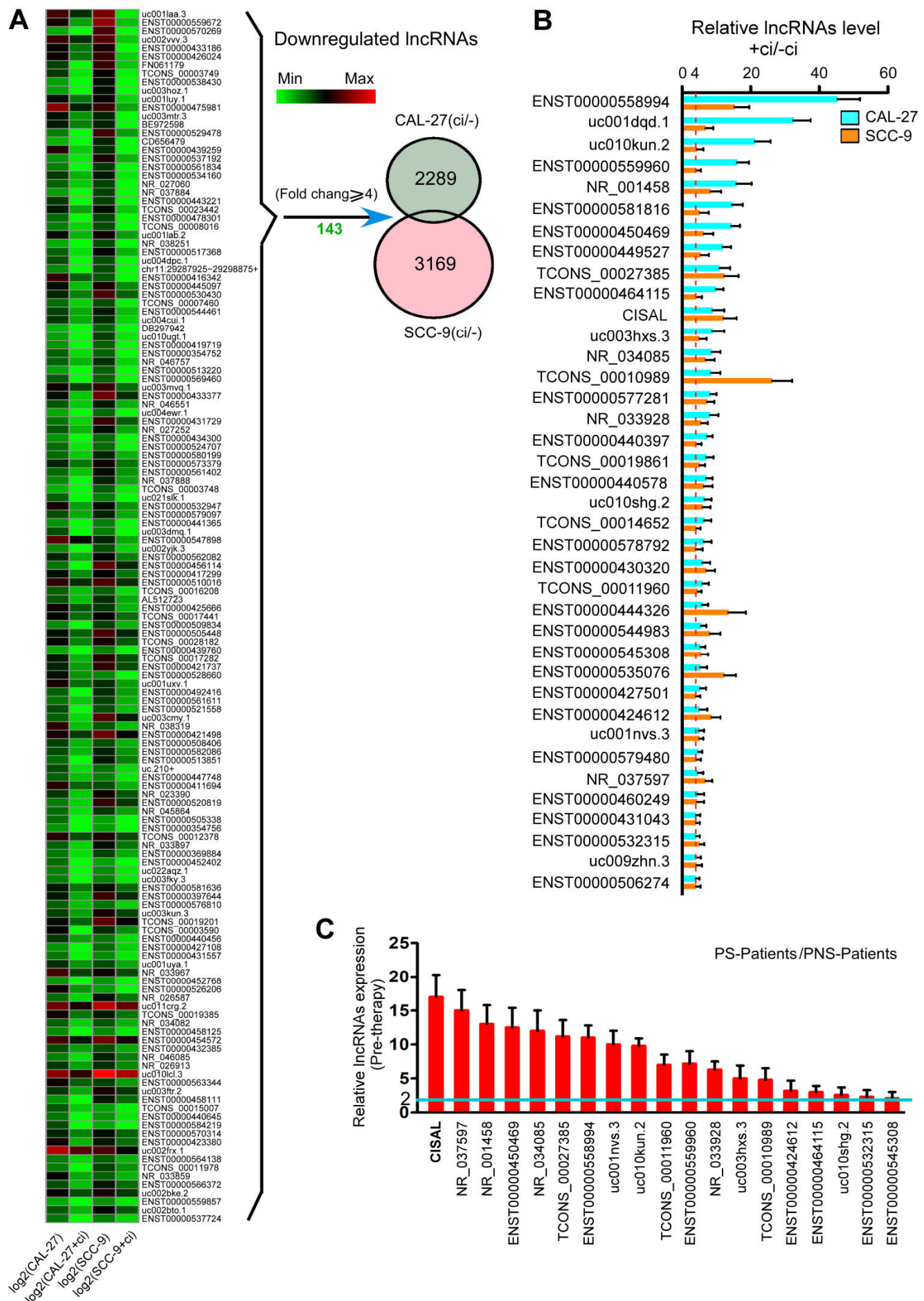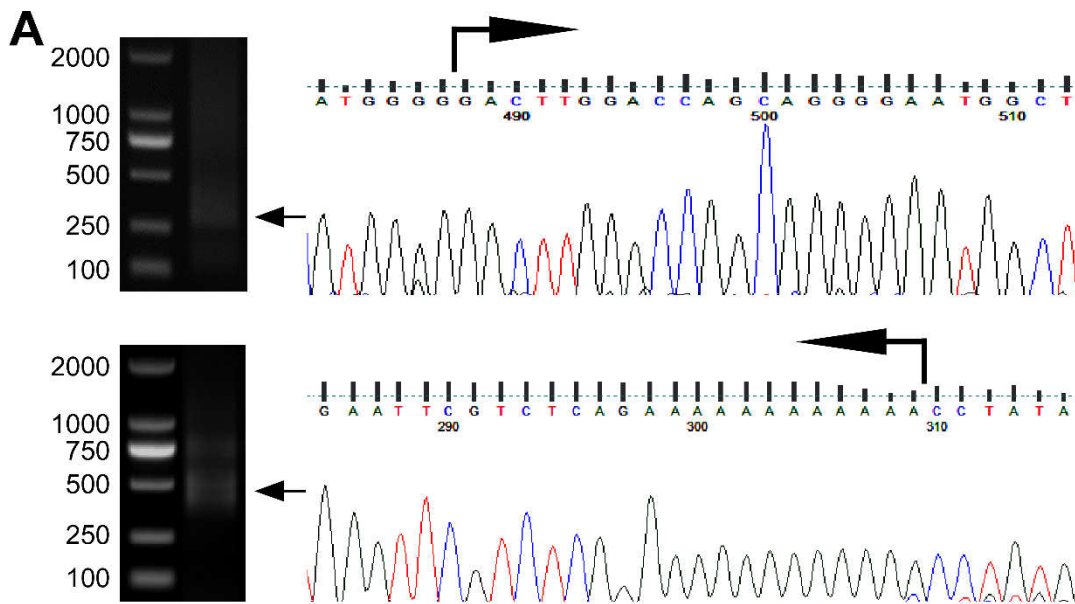
Figure S1. LncRNA profile and validation in TSCC cells and tumors. (A) Heat map showing 143 downregulated lncRNAs in two TSCC cell lines treated with cisplatin compared to untreated control. The

relative lncRNA expression is depicted according to the color scale. Green to red color gradation is based on the ranking of each condition from minimum (green) to maximum (red). (B) 38 upregulated lncRNAs were identified by qRT-PCR in both CAL-27 and SCC-9 cells treated with cisplatin compared to control. (C) Among 38 upregulated lncRNAs, 19 lncRNAs were validated to be increased in chemosensitive (PS) patients before neoadjuvant chemotherapy comparing to chemoresistant (PNS) patients by qRT-PCR. Related to Figure 1.
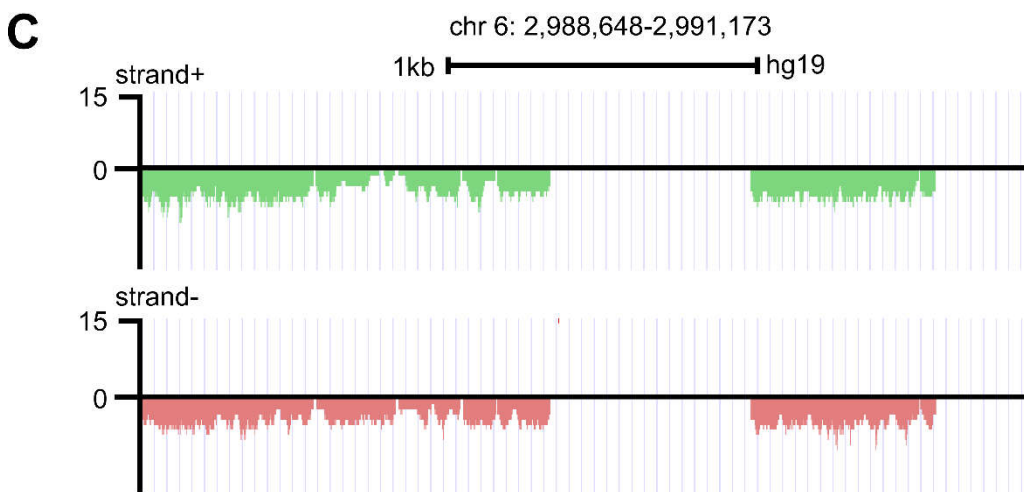
Figure S2. RACE assay of CISAL. (A) 5' RACE and 3' RACE of CISAL. Left: gel electrophoresis of nested PCR products from 5' RACE and 3' RACE. The arrow on the right indicates the major PCR product. Right: PCR product sequencing reveals the boundary between the universal anchor primer and CISAL sequences. The vertical line indicates a putative transcriptional start site or a putative transcriptional end site. Arrows indicate transcriptional directions. (B) Prediction of putative proteins encoded by CISAL using ORF Finder (https://www.ncbi.nlm.nih.gov/orffinder). (C) The codon substitution frequency (CSF) scores of CISAL. Related to Figure 1.
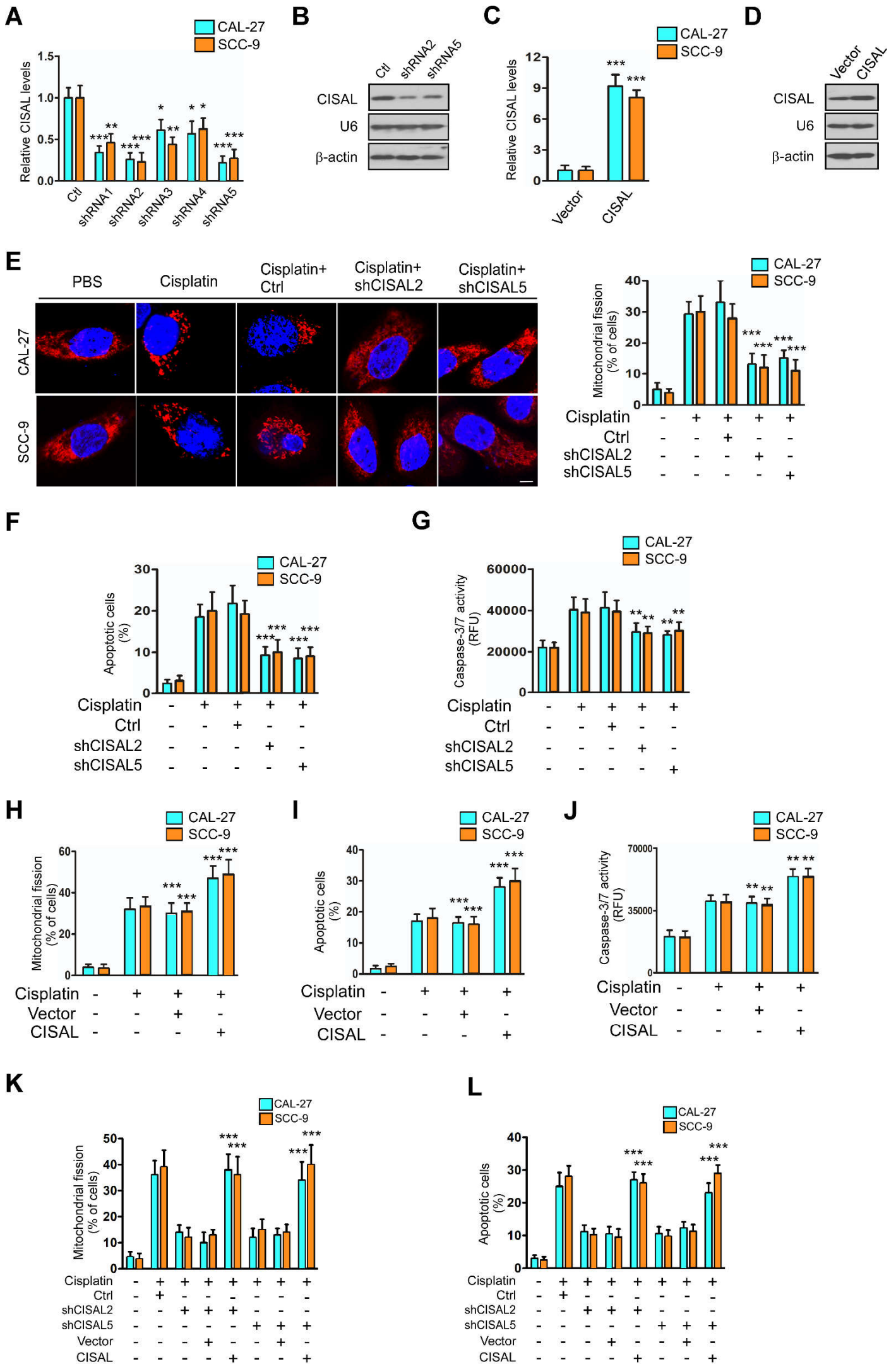
Figure S3. Regulation of CISAL expression in TSCC cells. (A) Knockdown efficiency of CISAL by different shRNAs in CAL-27 and SCC-9 cells. (B) Northern blotting demonstrates that CISAL probes specifically detect CISAL in CAL-27 cells. (C) CISAL expression in CAL-27 and SCC-9 cells with stable expression of CISAL. (D) Northern blotting revealed that overexpression of CISAL in CAL-27 cells resulted in a specific increase of CISAL levels. (E-G) CAL-27 and SCC-9 cells were treated with shRNA against CISAL. Mitochondrial fission was detected by staining with MitoTracker Red (left panel) and quantified (right) (E); cell apoptosis was detected using flow cytometry (F), and caspase-3/7 activity assays (G). (H-J) CISAL was overexpressed in CAL-27 and SCC-9 cells and mitochondrial fission (H), cell apoptosis (I) and caspase 3/7 activity (J) was detected. (K and L) The inhibitory effect of CISAL knockdown on mitochondrial fission (MitoTracker red) and apoptosis (flow cytometry) was abolished by CISAL overexpression. (M) CAL-27 and SCC-9 cells were treated with 2×10^{-6} M adriamycin (ADR) (Sigma, USA) or 15×10^{-6} M camptothecin(CPT) (Sigma, USA) for 24 hours to detect CISAL expression. *$P<0.05$, **$P<0.01$ and ***$P<0.001$ versus control, 2-tailed Student's t test; scale bar, 3 μm. Data are represented as mean ±SEM. Related to Figure 2.
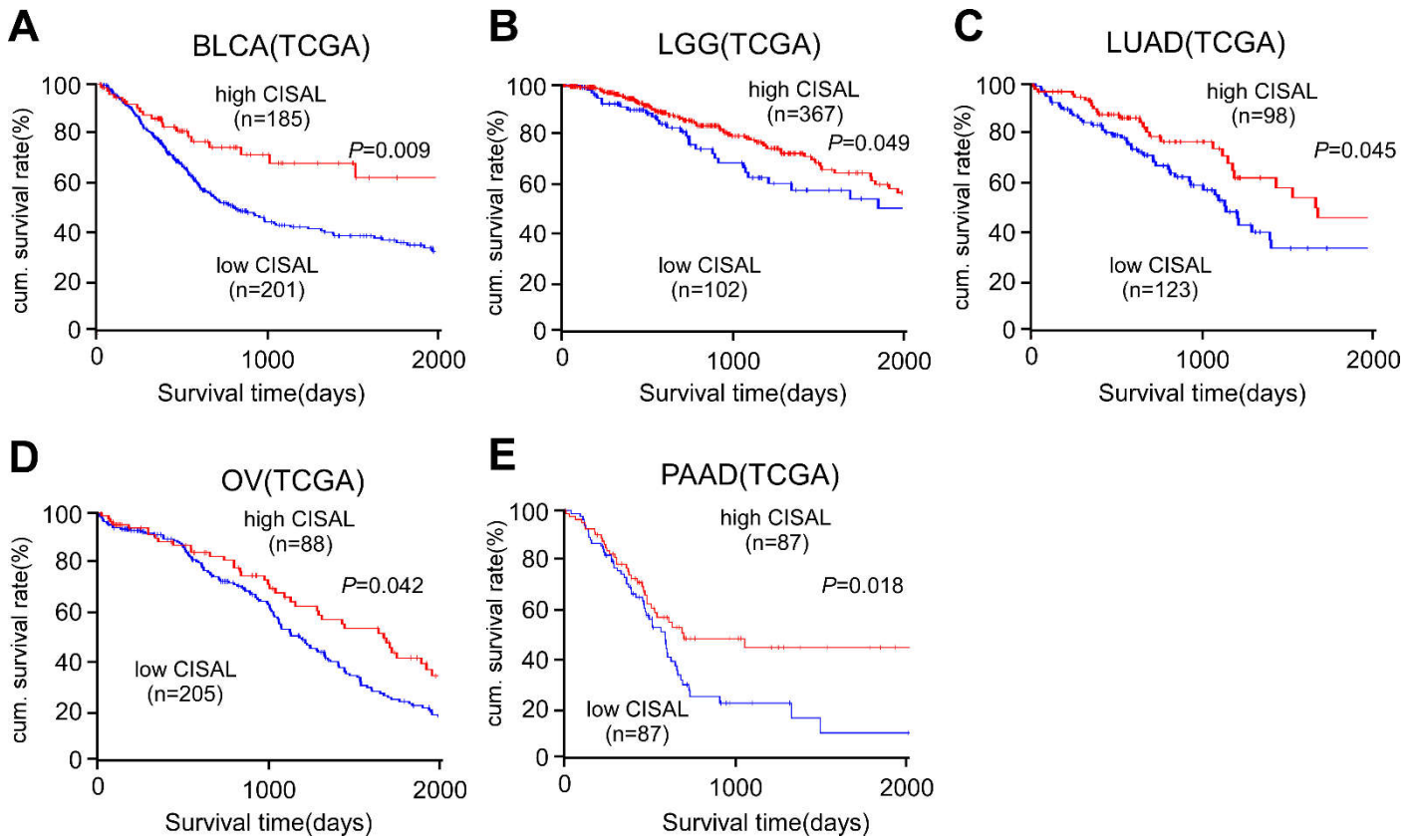
Figure S4. (A-E) TCGA data analysis showing higher CISAL expression is associated with better overall survival in multiple types of cancers including bladder carcinoma (BLCA) (A), low grade gliomas (LGG) (B), lung adenocarcinoma (LUAD) (C), ovarian cancer (OV) (D), and pancreatic adenocarcinoma (PAAD) (E). Related to Figure 2.
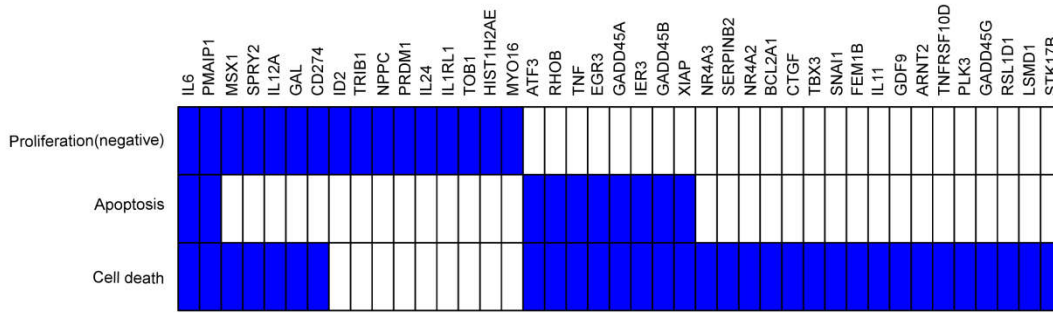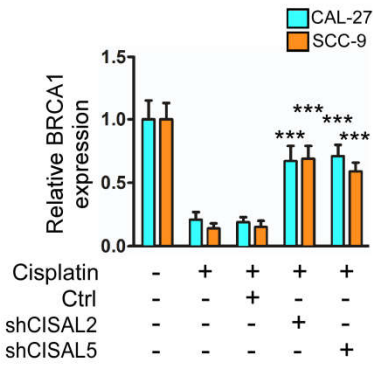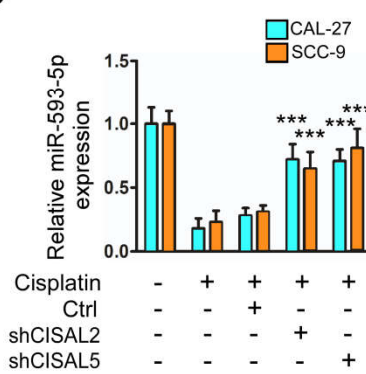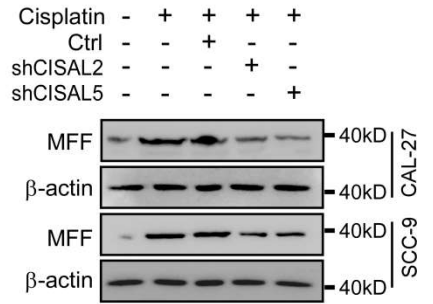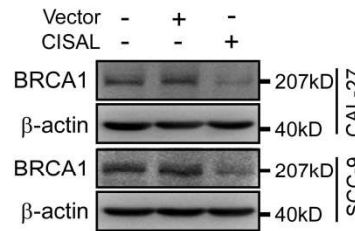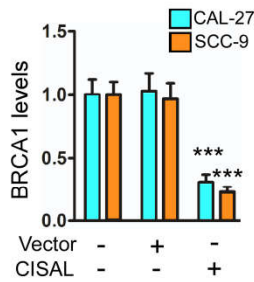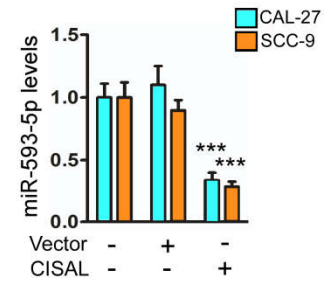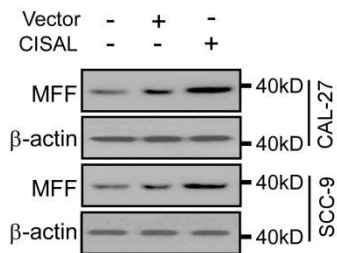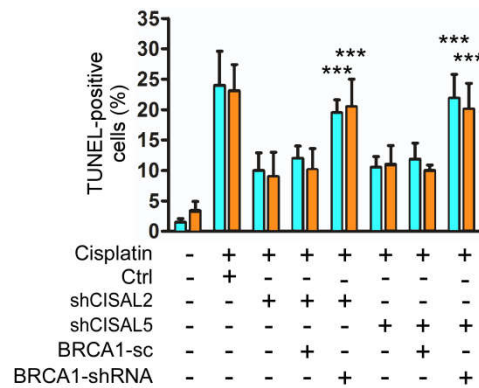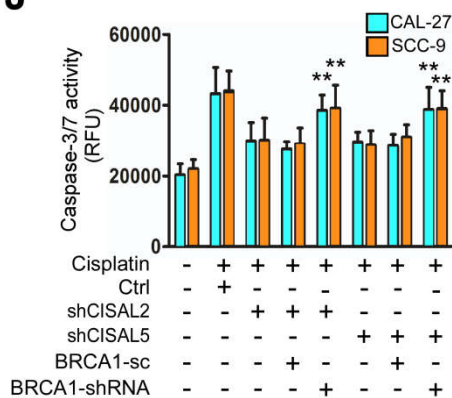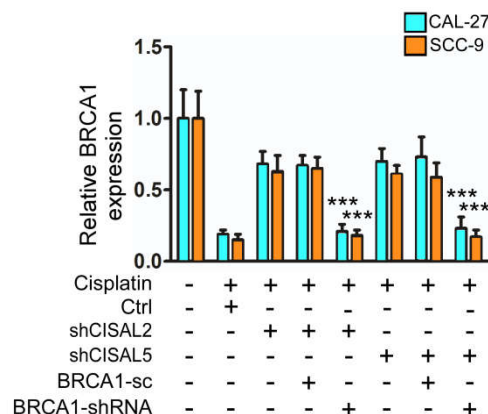
Figure S5. CISAL regulates BRCA1, miR-593-5p and MFF expression in TSCC cells. (A) Gene set enrichment analysis (GSEA) showing three significantly induced pathways associated with the genes downregulated upon CISAL knockdown in both TSCC cell lines under cisplatin treatment. (B) qRT-PCR showing that knockdown of CISAL expression increases BRCA1 in TSCC cells under cisplatin treatment. (C) miR-593-5p was upregulated upon CISAL silencing in TSCC cells under cisplatin treatment. (D) Western blotting indicating that MFF expression was downregulated upon CISAL knockdown in TSCC cells under cisplatin treatment. (E) qRT-PCR (left panel) and Western blot (right panel) demonstrating that CISAL overexpression results in reduction of BRCA1 expression in CAL-27 and SCC-9 cells. (F) Overexpression of CISAL downregulated miR-593-5p expression in both TSCC cell lines. (G) The MFF protein level was increased by CISAL overexpression in both TSCC cell lines. (H-I) The inhibitory effect of CISAL knockdown on mitochondrial fission, analyzed by TUNEL (H) and caspase-3/7 activity (I), after BRCA1 silencing. (J) qRT-PCR showing that the enhanced expression of BRCA1 by CISAL knockdown was attenuated upon silencing of BRCA1. **$P<0.01$ and ***$P<0.001$, 2-tailed Student's t test. Data are represented as mean ±SEM. Related to Figure 2.
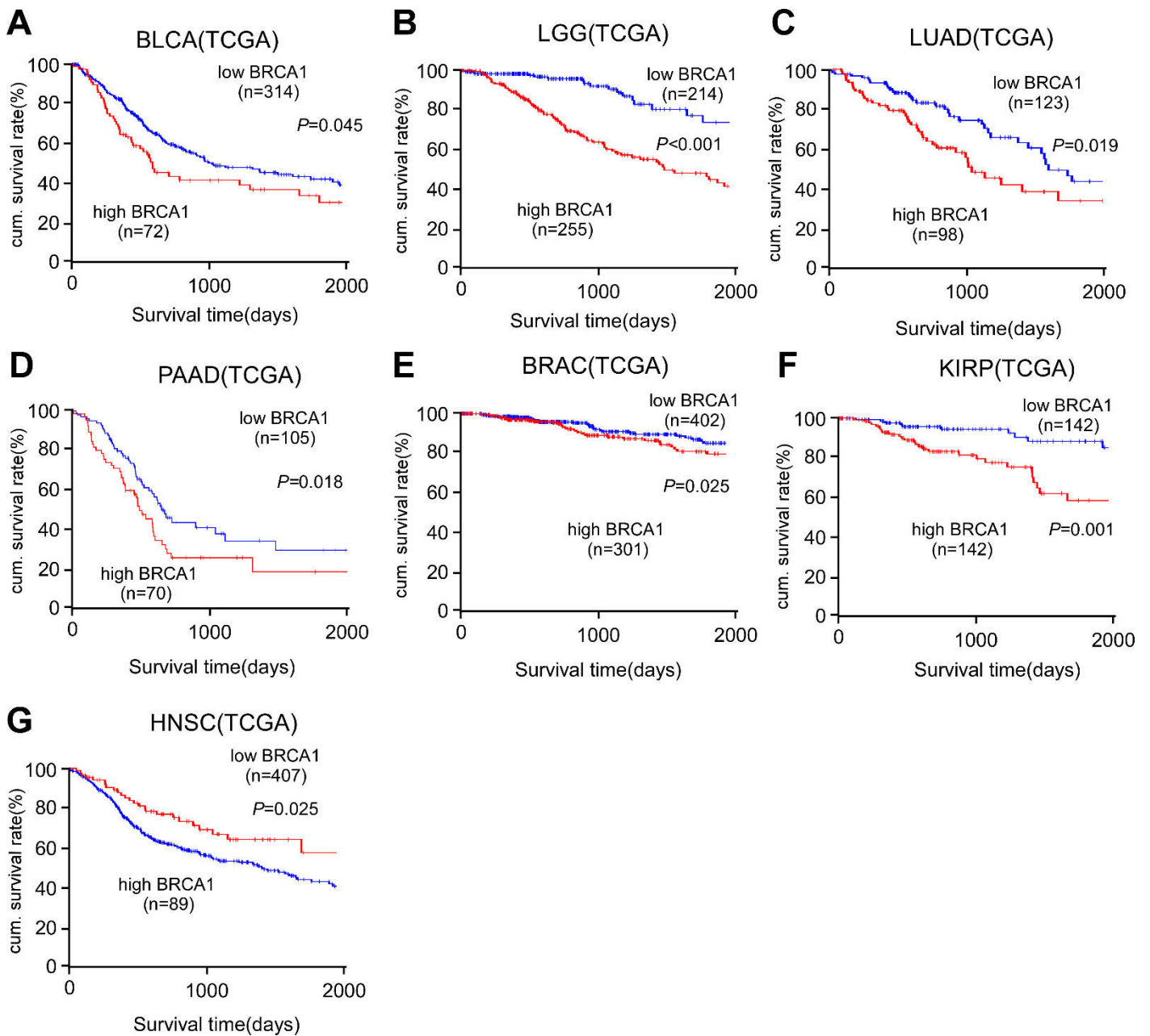
Figure S6. (A-G) TCGA data analysis showing that lower BRCA1 expression is associated with better overall survival in multiple types of cancer such as bladder carcinoma (BLCA) (A), low grade glioma (LGG) (B), lung adenocarcinoma (LUAD) (C), pancreatic adenocarcinoma (PAAD) (D), breast invasive carcinoma (BRAC) (E), kidney renal papillary cell carcinoma (KIRP) (F), head neck squamous cell carcinoma (HNSC) (G). Related to Figure 2.
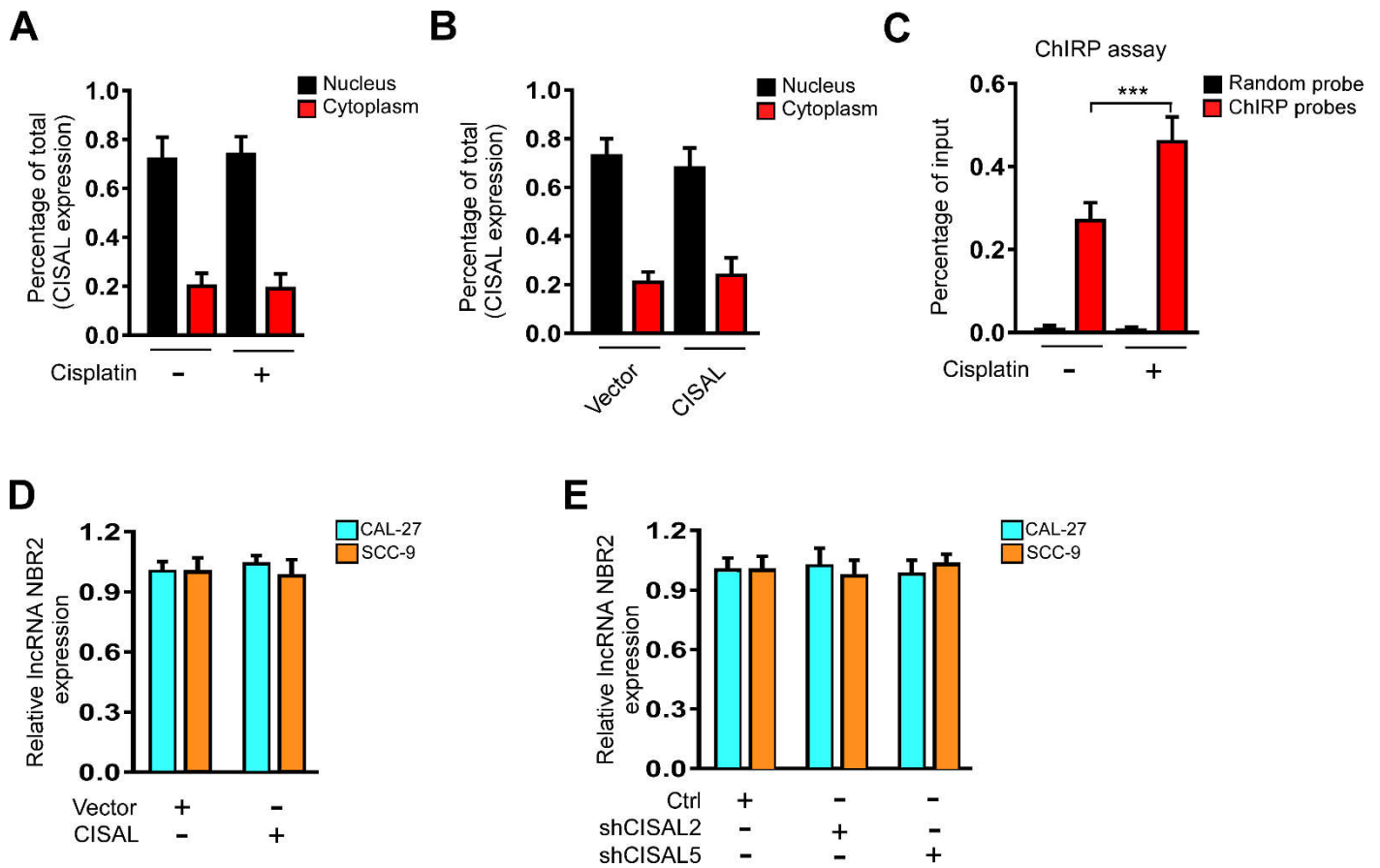
Figure S7. (A and B) CISAL distribution in cisplatin-treated CAL-27 cells (A) and untreated CAL-27 cells with stable CISAL expression (B). (C) ChIRP analysis of CISAL around the regulatory regions of BRCA1(-1627, -1606) in CAL-27 cells under cisplatin treatment. The crosslinked CAL-27 cell lysates were incubated with biotinylated DNA probes against CISAL, and the binding complexes were recovered using streptavidin-conjugated magnetic beads. qPCR was performed to detect enrichment of the specific regulatory regions associated with CISAL. (D and E) lncRNA NBR2 levels were detected by qRT-PCR in CAL-27 and SCC-9 cells with CISAL overexpression (D) or knockdown (E). ***$P<0.001$, 2-tailed Student's t test. Data are represented as mean ±SEM. Related to Figure 3.
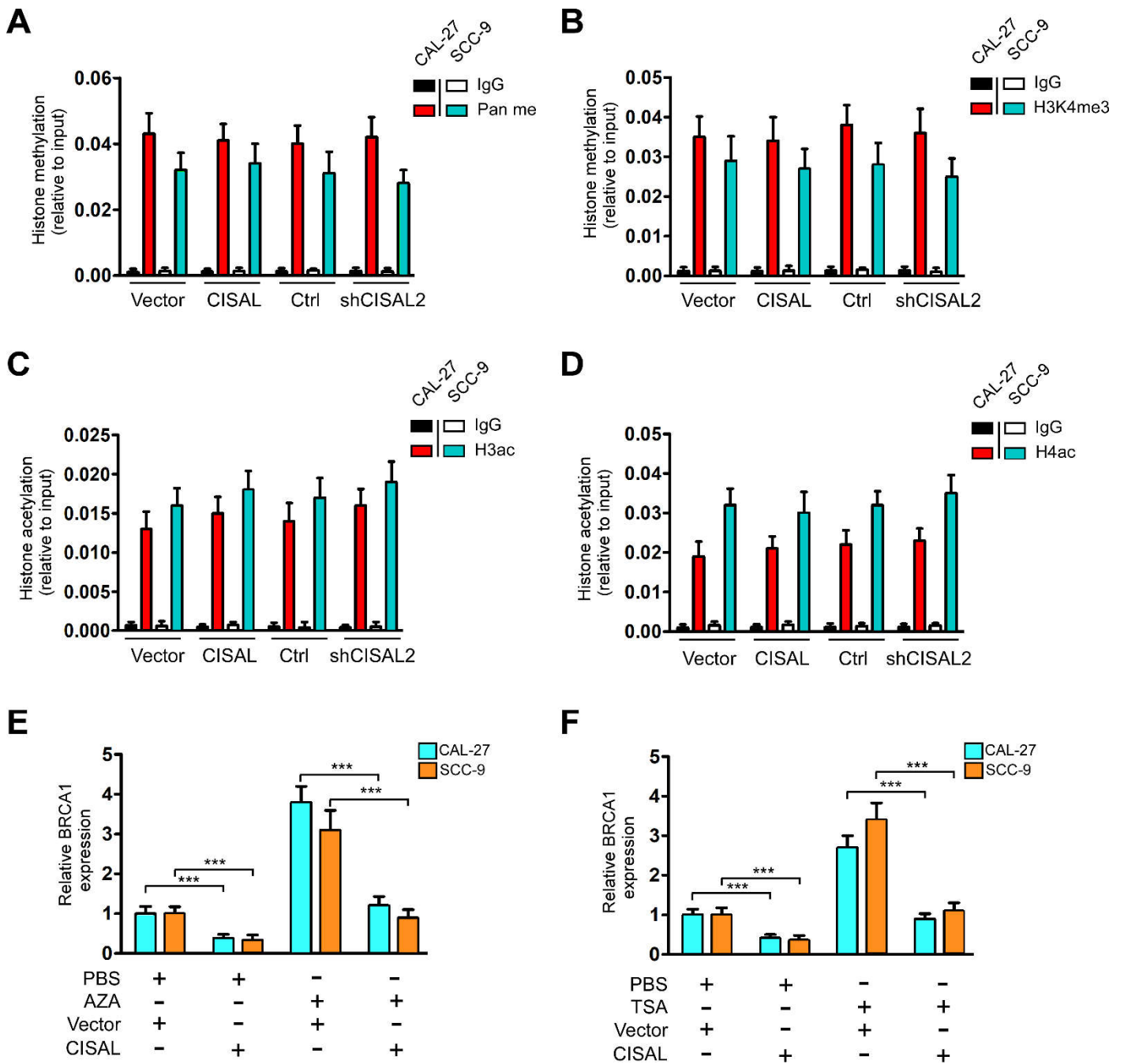
Figure S8. CISAL has no effect on histone methylation and deacetylation at BRCA1 promoter. (A and B) The pan-histone H3 methylation (Pan me) and H3K4 methylation (H3K4me3) at BRCA1 promoter regions were analyzed by ChIP-qPCR assay in CAL-27 and SCC-9 cells. (C and D) The histone H3 acetylation (H3ac) and histone H4 acetylation (H4ac) at BRCA1 promoter regions were analyzed by ChIP-qPCR assay in CAL-27 and SCC-9 cells. The histone modification in 10% input DNA was set to 1. IgG was used as a negative control. (E) CISAL overexpression reduced BRCA1 expression upon 5-aza-dC treatment. (F) CISAL overexpression reduced BRCA1 expression under TSA treatment. ***$P<0.001$, 2-tailed Student's t test. Data are represented as mean ±SEM. Related to Figure 4.
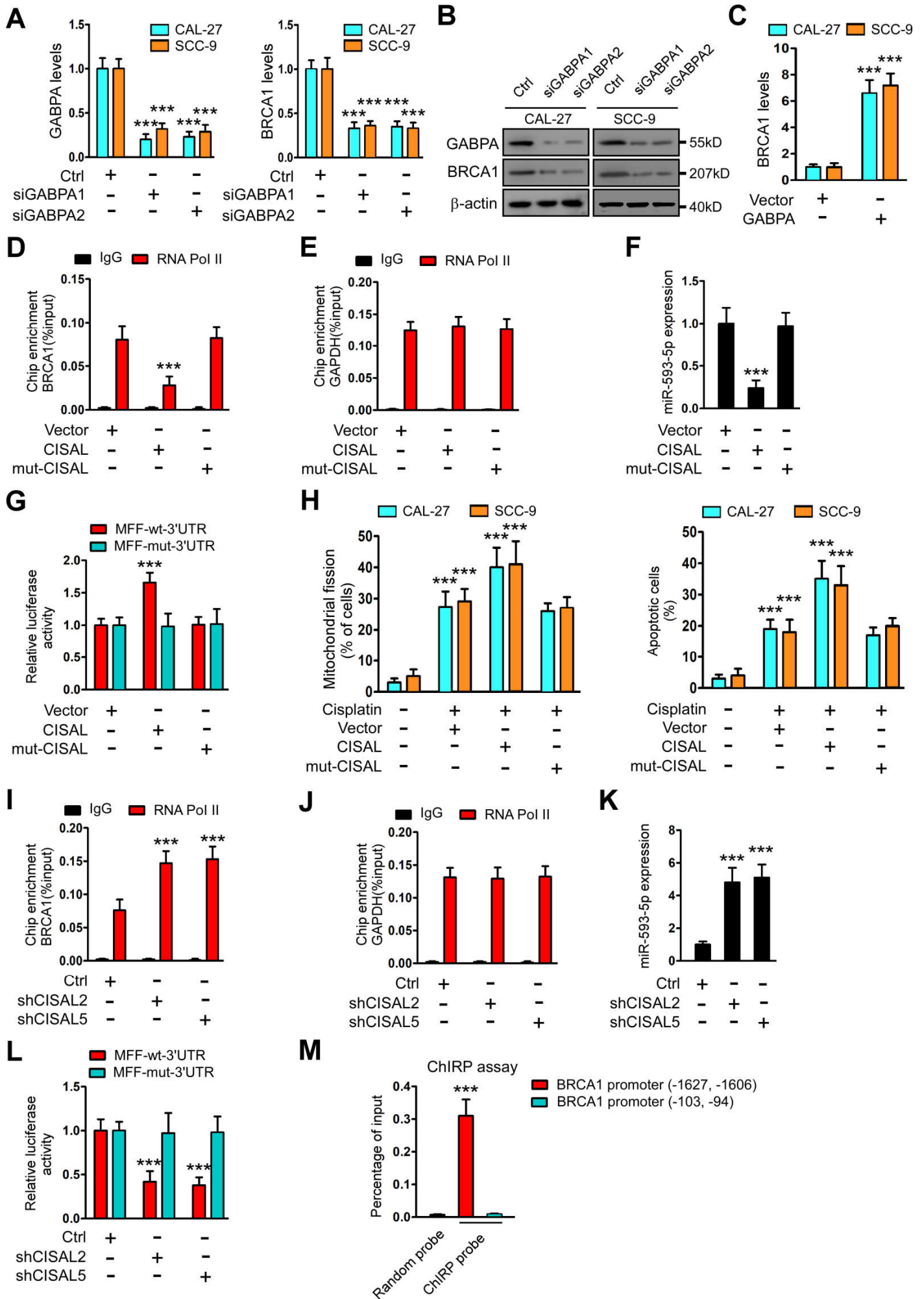
Figure S9. CISAL modulates BRCA1-miR-593-MFF axis through transcriptional regulation of BRCA

expression. (A and B) qRT-PCR (A) and Western blotting (B) showing that knockdown of GABPA significantly reduces GABPA and BRCA1 expression in CAL-27 and SCC-9 cells. (C) BRCA1 expression in CAL-27 and SCC-9 cells with stable GABPA expression. (D and E) ChIP-qPCR analysis of RNA pol II occupancy in the BRCA1 (D) and GAPDH (E) promoter after overexpression of CISAL or mutant CISAL (mut-CISAL) in CAL-27 cells. (F) Forced expression of mut-CISAL failed to inhibit miR-593-5p levels in CAL-27 cells. (G) Luciferase reporter assay demonstrating overexpression of CISAL but not its mutants reduces miR-593 functionality in CAL-27 cells. (H) Mutant CISAL failed to enhance mitochondrial fission and cell apoptosis in CAL-27 and SCC-9 cells. (I and J) ChIP-qPCR analysis of RNA pol II occupancy in the BRCA1 (I) and GAPDH (J) promoter in CAL-27 cells with CISAL knockdown. (K) Knockdown of CISAL expression increases miR-593-5p levels in CAL-27 cells. (L) Luciferase reporter assay showing that CISAL knockdown enhances miR-593 functionality in CAL-27 cells. (M) ChIRP analysis showing CISAL in the regulatory regions of BRCA1 promoter (-1627, -1606) but not (-103, -94). The crosslinked CAL-27 cell lysates were incubated with biotinylated DNA probes against CISAL, and the binding complexes were recovered using streptavidin-conjugated magnet beads. qPCR was performed to detect enrichment of the specific regulatory regions associated with CISAL. ***$P<0.001$, 2-tailed Student's t test. Data are represented as mean ±SEM. Related to Figure 4.
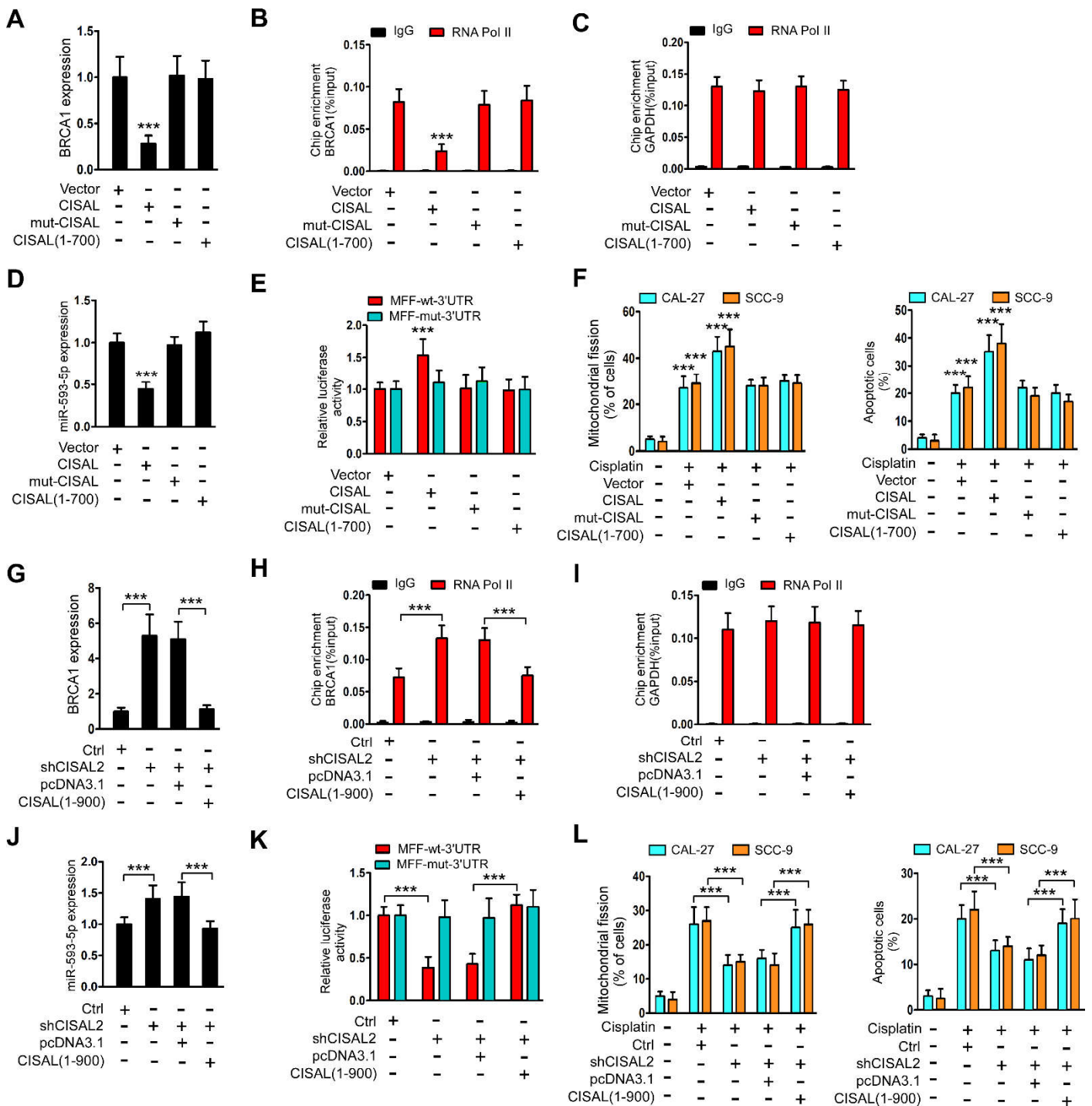
Figure S10. CISAL determines BRCA1 transcription, mitochondrial fission and cell apoptosis in TSCC cells. (A) Site-directed mutagenesis of 1–700 nt of CISAL leads to a loss of the effect on BRCA1 levels in CAL-27 cells. (B and C) ChIP-qPCR analysis demonstrating that forced expression of truncated CISAL (1–700) had no effect on RNA pol II occupancy in the BRCA1 (B) and GAPDH (C) promoter in CAL-27 cells. (D and E) Overexpression of CISAL (1–700) lost ability to inhibit miR-593-5p expression (D) and the functionality (E) in CAL-27 cells. (F) Mitochondrial fission and apoptosis were detected in both CAL-27 and SCC-9 cells with transduction of site-directed mutagenesis of 1–700 nt of CISAL. (G) Forced expression of the truncated CISAL (1–900) abolished the increase of BRCA1 levels in CAL-27 cells. (H and I) ChIP-qPCR analysis showing that forced expression of the truncated CISAL(1–900) abolishes the increase of RNA pol II occupancy in the BRCA1 (H) but not GAPDH (I) promoter by depletion of endogenous CISAL in CAL-27 cells. (J and K) qRT-PCR (J) and luciferase assays (K) demonstrating that

forced expression of CISAL(1–900) attenuates the increase of miR-593-5p levels and functionality by depletion of endogenous CISAL in CAL-27 cells. (L) Forced expression of the truncated CISAL (1–900) abolished the decrease of mitochondrial fission and apoptosis in both CAL-27 and SCC-9 cells by silencing endogenous CISAL. ***P<0.001, 2-tailed Student's t test. Data are represented as mean ±SEM. Related to Figure 5.
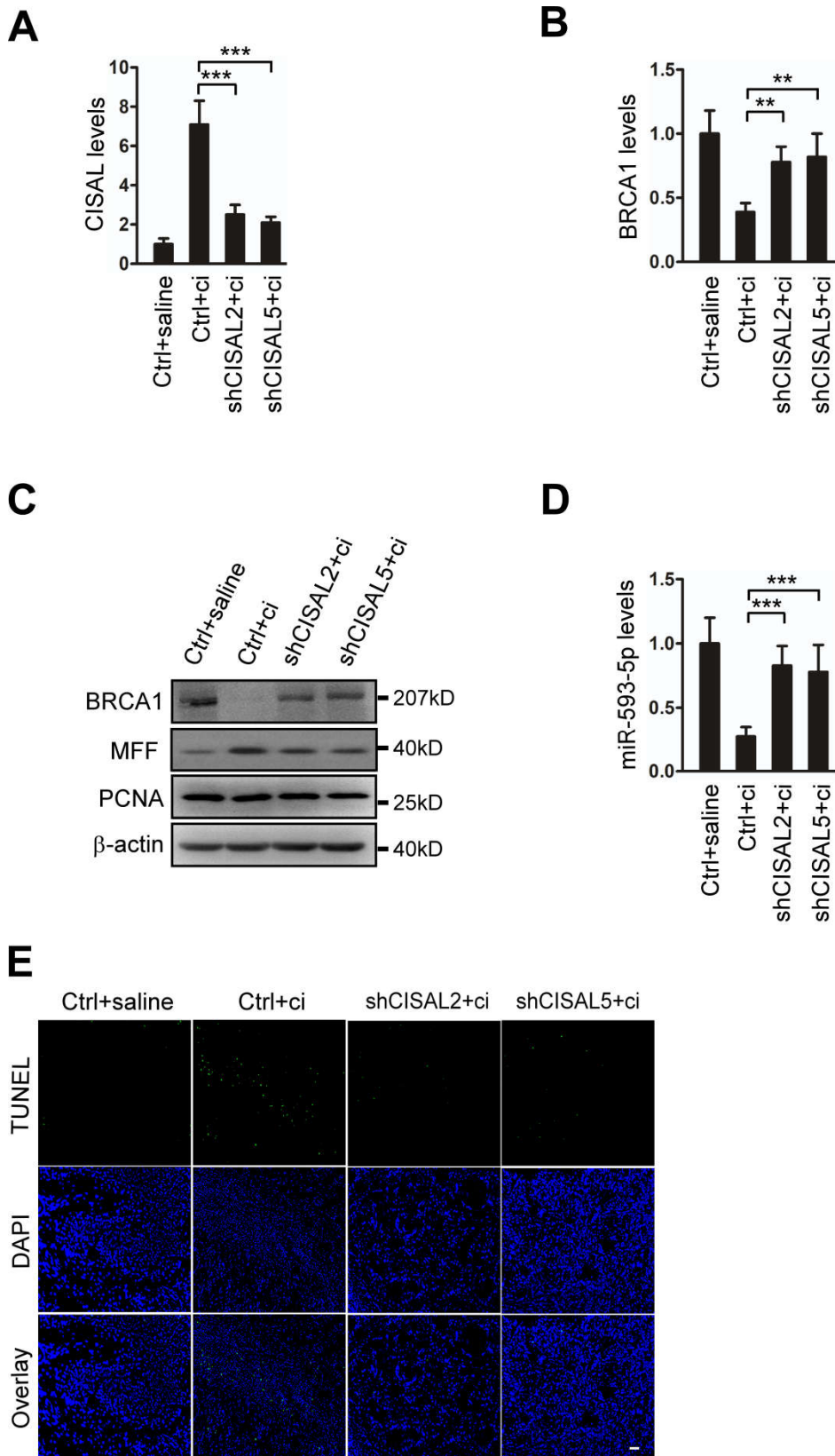
Figure S11. CAL-27 xenograft with CISAL knockdown in BALB/c nude mice. (A) qRT-PCR showing CISAL expression in each group. (B) qRT-PCR showing that BRCA1 expression was increased by CISAL knockdown. (C) Western blot indicating that BRCA1 expression was increased, but MFF was downregulated, upon silencing CISAL in TSCC xenograft treated with cisplatin, while PCNA was not changed in any group. (D) qRT-PCR showing that miR-593-5p expression was upregulated upon CISAL knockdown. (E) TUNEL assays showed that apoptosis in response to cisplatin was attenuated by CISAL knockdown. scale bar, 20 μm.**P<0.01 and ***P<0.001, 1-way ANOVA followed by Dunnett's tests for

multiple comparisons. Data are represented as mean ±SEM. Related to Figure 6.
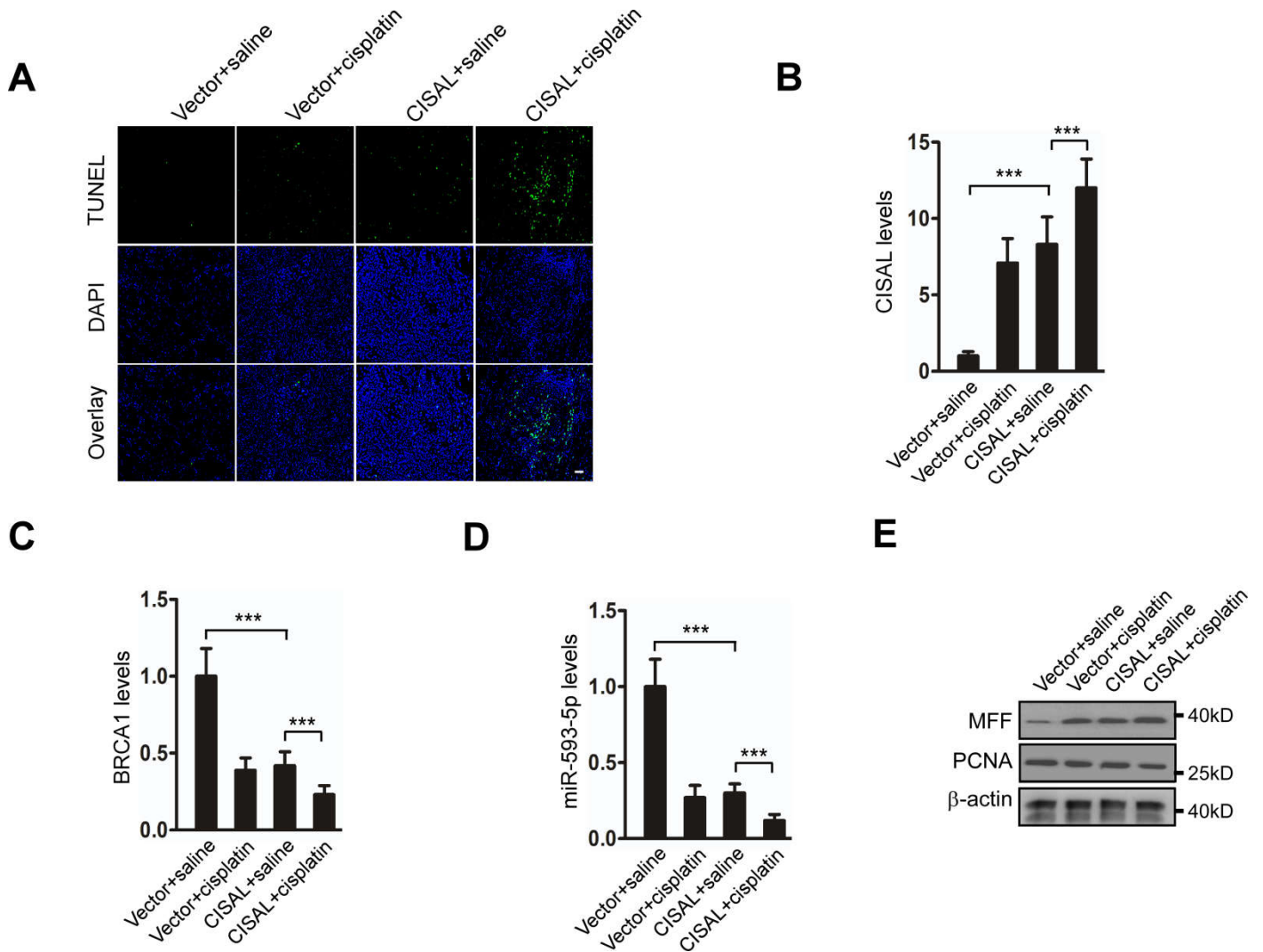
Figure S12. CISAL overexpression increases apoptosis and cisplatin sensitivity in CAL-27 xenografts in vivo. (A) BALB/c nude mice bearing xenografts of CAL-27 cells with stable CISAL expression or control vector were treated with saline or cisplatin (n=6 per group). TUNEL assay showing that apoptosis in response to cisplatin was attenuated upon CISAL knockdown; scale bar, 20 μm. (B-E) CISAL (B), BRCA1 (C), miR-593-5p (D), MFF and PCNA (E) expression in each group. ***$P<0.001$, 1-way ANOVA followed by Dunnett's tests for multiple comparisons. Data are represented as mean ±SEM. Related to Figure 6.
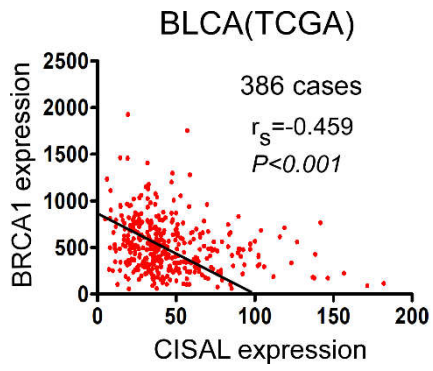
Figure S13. TCGA data analysis showing that CISAL levels reversibly correlates with BRCA1 expression in bladder carcinoma (BLCA). Related to Figure 7.

Supplemental Tables

Table S1. Clinical characteristics of TSCC patients. Related to Figure 1.

Patient ID	Age (years)	Gender	Pathological diagnosis	TNM stage	NaC	Cycles	Responses
PS 1	69	F	TSCC	T4N1M0	TPF/TPF	2	Partial
PS 2	56	F	TSCC	T3N0M0	TPF	1	Partial
PS 3	43	F	TSCC	T4N1M0	TPF/TPF	2	Partial
PS 4	73	M	TSCC	T3N1M0	TPF	1	Partial
PS 5	66	F	TSCC	T3N0M0	TPF/PF	2	Partial
PS 6	54	F	TSCC	T3N1M0	TPF/TPF	2	Partial
PS 7	41	M	TSCC	T3N0M0	TPF/TP	2	Partial
PS 8	77	M	TSCC	T4N2M0	TPF	1	Partial
PS 9	59	F	TSCC	T3N0M0	TPF/TPF	2	Partial
PS 10	68	M	TSCC	T3N1M0	TPF	1	Partial
PS 11	71	F	TSCC	T4N1M0	TPF/TP	2	Partial
PS 12	54	M	TSCC	T4N2M0	TPF	1	Partial
PS 13	39	M	TSCC	T3N1M0	TPF/TP	2	Partial
PS 14	48	F	TSCC	T4N2M0	TPF/TP	2	Partial
PNS 1	54	M	TSCC	T3N0M0	TPF/TPF	2	Progressive
PNS 2	67	F	TSCC	T3N2M0	TPF	1	Stable
PNS 3	48	M	TSCC	T3N1M0	TPF/TPF	2	Progressive
PNS 4	49	F	TSCC	T4N2M0	TPF	1	Progressive
PNS 5	35	F	TSCC	T3N0M0	TPF/TPF	2	Stable
PNS 6	55	M	TSCC	T4N1M0	TPF	1	Stable
PNS 7	39	F	TSCC	T3N0M0	TPF	1	Progressive
PNS 8	41	F	TSCC	T3N1M0	TPF/PF	2	Stable
PNS 9	67	M	TSCC	T3N1M0	TPF/TPF	2	Stable
PNS 10	59	M	TSCC	T3N0M0	TPF/TPF	2	Progressive
PNS 11	68	M	TSCC	T4N2M0	TPF	1	Stable
PNS 12	69	F	TSCC	T3N0M0	TPF/TPF	2	Progressive
PNS 13	74	M	TSCC	T3N0M0	TPF/TPF	2	Stable
PNS 14	53	M	TSCC	T4N0M0	TPF	1	Stable
PNS 15	47	F	TSCC	T4N2M0	TPF/PF	2	Stable

PS, patient with partial response; PNS, patient with progressive or stable disease; TSCC, tongue squamous cell carcinoma; NaC, neoadjuvant chemotherapy; TP, docetaxel+cisplatin; PF, cisplatin+ 5-fluorouracil; TPF, docetaxel+cisplatin+5-fluorouracil;

Table S2. The full-length nucleotide sequence of CISAL. Related to Figure 1.

GACTTGGACCAGCAGGGGAATGGCTGTGACAATAAATAAGATTGGGAAAACAAGAAGACGCCC
TTGCATACATTAAGATATGTATATATGGAAATGTTACCGGGAGTCCCGGTTATCCCAAAAAGGGTT
GTTTCCTGTTGCGTGGTGAGGCCAATGCACGAAACCGAAAGGGAGTGTGTCAAGCAGTGCAGG
CTGTATTCAATGGCTATGGAATTGGAAGATCTGAAATCAACTTAGCTTGTGAGAGCTGGGAAGTT
TCAGAGTCGTTGTCATGGCGACATGTTGTTTAGCATGAGAACAGGATGATGATAAAGCCAGAGG
CTCTTCAGAGGCGCCATCTTGGATTTCGCCAGCTTCAGCTGGTTTCGTCCTAAGAAGGAACTTCG
AAACACAGGCATTCTTTTTCCTGAAAATAAGCAGAGTTACAGCTGAGTAGGAATTTAGCTCTGTC
CCATATGCTATCGCATTGGGCAGCAAAGCAGGGTGGGGTCCAGCGAAATCAGCAGGCACTGCA
ATGAGTAACATACCCAGCCACGTTTATGCAGCATTTTTACGAAAATGAAACCATACTACCTGTAA
AGGAAGATATGCTAACAAACAACAAAACTGGCAGGAACCAAGATTCCTACTGACACTACCCTTA
GTTTTAATTTTCCCTGACAACAAATGAGGTTAACAGAGCATAATTATCTACCGTGACCCCTTCAA
AAAGACAGGCTGTATACATTTGCACTAAGAGAAGAAATCGTGTAATGTCAGCAAATTTCCCCCA
CTTAAAGCTTCTCTATTTAAAAAGCTTCACGCACACATGCACGCATATGTCTTCAAGATGACCAC
AATTTATTTTGCAGTCATTCTTTGCACCAGTTCCCAATTTTTCCCACTAGCTTGCAAGCTCCGTGA
CTCGAGGAGACCGGGGGATCAGAGTTTGTTTTTGCGGAGAAGTGAGTCCTTTATGCCCCAAATA
GTGACTGACATAGAGAAGGTACTCAGTAAACACTTTTTAAAGGAATGCCTGCCTGACTGAAGCT
TAATGATGTGAGGCTTCTAGTGGGATACCCTACCTTGTTTTAACCTGAAGTGACTCTTCCTTAGCT
AAGAGAGCCAGACGGACTCCATCGTGACTCCTTCACTCGCAGCCCCTTACCCACCCCCTTCCTC
AAGGACTTAACTTGTGCAAGCTGACTCCCAGCACATCAAGAATGCAATTAACTGATAAGATACT
GTGGCAAGCTATATCCGCAGTTCCCAGGAATTCGCCCGGTTAATAGCACCCAGAGCCCCTGCGTT
TGTGTCCGGTTGATAACGCCCAAAGCCCGGCGTCCATCACCTTAGGATAGACTTAAAGCCTCTGC
ACCTGGAACTGTTTACTTTCCTGTAACCGTTTATCCTTTTAACTTTTTGCCTACTTTACTTCTGTAA
GATTGTTTCAACTAGACTCCCCCTCTCCCCTGTCTAAACCAAAGTATAAAAGAAAATCTAGCTCC
TTCTTCGGGGCCAAGAGAATTTCGAGCGCTAGCTGTCTCTCGGCTGCCGGCTAATAAAGGACTC
CTGAATTCGTCTCAGAAAAAAAAAAAAAAAAA

Table S3. Correlation among clinicopathological status and the expression of CISAL and BRCA1 in TSCC patients. Related to Figure 7.

Characteristics	CISAL (%)		P	BRCA1(%)		P
	No. of low Expression	No. of high Expression		No. of low Expression	No. of high Expression	
Sex			0.770			0.234
Male	26(41.9)	36(58.1)		42(67.7)	20(32.3)	
Female	20(39.2)	31(60.8)		29(56.9)	22(43.1)	
Age			0.980			0.120
$<$50	15(40.5)	22(59.5)		27(73.0)	10(27.0)	
$\geq$50	31(40.8)	45(59.2)		44(57.9)	32(42.1)	
Node metastasis			0.959			0.329
N0	19(40.4)	28(59.6)		32(68.1)	15(31.9)	
N+	27(40.9)	39(59.1)		39(59.1)	27(40.9)	
Clinical stage			0.845			0.232
III	28(40.0)	42(60.0)		41(58.6)	29(41.4)	
IV	18(41.9)	25(58.1)		30(69.8)	13(30.2)	
Cisplatin			0.009			$<$0.001
Sensitive	18(29.5)	43(70.5)		48(78.7)	13(21.3)	
Non-sensitive	28(53.8)	24(46.2)		23(44.2)	29(55.8)	
Status (60 months)			0.018			0.008
Survival	10(25.6)	29(74.4)		31(79.5)	8(20.5)	
Death	36(48.6)	38(51.4)		40(54.1)	34(45.9)	

Table S4. Primers used in this study. Related to Figure 1.

Gene	Forward primer (5'-3')	Reverse primer (5'-3')
qRT-PCR		
NR_033928	TTCTTTCACCATTTCACACA	AACCCTACCTGGACACATC
TCONS_00019861	CAGAGAATGCGTGAATGG	TTGAGGGAAGGGGAGTAA
TCONS_00014652	GCTTTCTTTCACCATTTCAC	GGACACATCATAGTCATCATACA
ENST00000558994	GACGGGAATGAAAGAAGA	CAGAGAGGTGGAGGGACT
CISAL	CGAAACCGAAAGGGAGTG	CATGTCGCCATGACAACG
NR_034085	GCAGTATGAAAATGGCTAGAGATTG	GGCTCTACATCATTTGTCGTATGTG
ENST00000449527	ACTTTCTTCAGTCACATCTGAA	CGCCAATGGGTGAAATCTAAAG
uc003hxs.3	AGGCGTAAGAAACCTCCT	TTCATCAGAGTCCCTCCA
NR_001458	GAACAACCTACCAGAGACCTT	CACAGATTTCCCCTTCCT
uc001dqd.1	TACACCCTTGAATCCCCTCTT	TCCATTGTTCCCTAACGACC
uc010kun.2	TCATCCATTCTTCACCGA	CATTTTCATTTTCACACCAA
ENST00000450469	GCCTGTGGGTAGATTTGA	TGTATTTTGATGACCTCTGCT
ENST00000581816	AACTCAAACCCCTTTCTACAC	ATCCCCACCAAACTCAAC
ENST00000559960	GTTCCAGCATAAAGTGAAAGA	AAGACAGCAAAACCAAAGAG
TCONS_00010989	GAAAGGAAGAAGGGAGAGAA	AGGATTACAGGCGTGAGC
TCONS_00027385	TCTATTTTGTCTCACCAGCAC	GCCTCAGTTTCCCTCACT
ENST00000578792	AAAATCAGGACGGAAAGG	CGACCCAGACTATTGGAG
ENST00000440578	ACGAGGTGGGAAGAAAAC	GAGAACAAAACAGTGAACAGAG
ENST00000440397	GCTTGTTTGGTTTCTGATAGTT	CCTCCTCTCCCTGGTATG
ENST00000464115	CGAGATGGTGGTGAATGT	AGTCCGAAGCGAGAGAAG
ENST00000577281	CACCCTCATCCCACTCTC	CCCACCATCTCACTTTCA
NR_037597	ATTTGTGTGTTGGATGGTG	CTTGATTTTGGACTTGTGG
uc010shg.2	CAAAAGATAAAGATGAACAGGAA	AAAGGAAGGAACAACCACTC
ENST00000424612	AGGAAACAAAAGCAAAACTG	GCCAGGAATAAAGCGAAG
ENST00000430320	AACTTTTATCAGCGGCAGT	GTTGGCTTCCATCTTGTG
TCONS_00011960	AGCACTGGACACACAAGAG	ATCACAGACCACAGCAGAA
ENST00000444326	TCATAGAGCCCAGAACAAA	GAAGCACAACCAGATAGAAAA
ENST00000545308	CTGCCTCCCAGGGTGAAT	ATGGATGAGGGTAACAGCACA
ENST00000579480	AGGGAGGTTGCTGATTCT	AGTTGGTTATGGGCGTGT
ENST00000460249	CCTGTCCTTACTCCCTCTTT	GGCTTACCTTCTCTTGGG
ENST00000544983	CCGTGAGGATAAATAACTCTG	GACAGGAGCCCAATAAGAC
uc001nvs.3	CCAGAACCCAAACTCAGG	ACAGAGGAACAGACACGAAG

ENST00000427501	GTTCTGAGTGTGGACGAGTAG	AGGTAATGCTAAAAGGCAAGT
ENST00000535076	CCAGAACCCAAACTCAGG	ACAGAGGAACAGACACGAAG
ENST00000532315	CCTCTGTCTGTCCTGCCT	CAGTCTCTTCAGTCTTTGTCCT
ENST00000431043	GTTCTGAGTGTGGACGAGTAG	AGGTAATGCTAAAAGGCAAGT
uc009zhn.3	CAAAAGATAAAGATGAACAGGAA	AAAGGAAGGAACAACCACTC
ENST00000506274	TTAGCGACATCAGGAAGAAC	CAAAGGAAGAGGGGACTG
BRCA1	GGCTATCCTCTCAGAGTGACATTTTA	GCTTTATCAGGTTATGTTGCATGGT
lncRNA NBR2	GGAGGTCTCCAGTTTCGGTA	TTGATGTGTGCTTCCTGGG
U6	CTCGCTTCGGCAGCACA	AACGCTTCACGAATTTGCGT
β-actin	AGCCTCGCCTTTGCCGATCC	ACATGCCGGAGCCGTTGTCG
Plasmid construction		
pcDNA-GABPA	ATAGGTACCATGACTAAAAGAGAAGCAGAGGAG	ATTGCGGCCGCTCAATTATCCTTTTCCGTTTGC
pcDNA-CISAL-wt	AAGGATCCAGACTACTGACTTGGACCAGCA	TCGATATCCTGAGACGAATTCAGGAGTCCT
pcDNA-CISAL-mut	ATCGTGACTCCTTCAAGACAUCAGAGGAUGAGUGCCCCTTCCTCAAGGAC	GTCCTTGAGGAAGGGGCACTCATCCTCTGATGTCTTGAAGGAGTCACGAT
pGL3-BRCA1	TGTGGTACCTGCATTTGCAAACCTTGAGC	TACTCGAGAGAGGGTGAAGGCCTCCTGA
EMSA		
BRCA1-70	GGGAGGCTCAGGCCACGCT	AGGACCTGCAGCCCGCCA
BRCA1-120	GCGCTGAGGAGCAGGGG	CCCTGCACAGGGCAAGGCT
ChIP-qPCR		
BRCA1(Histone Me/Ac)	AGGGCAGGCACTTTATGGC	CGCAGTCGCAGTTTTAATTTATC
BRCA1-GABPA	AGGGCAGGCACTTTATGGC	TACGAAATCAAGGTACAATCAGAGG
GAPDH	GACCTTCTTGCCTTGCTCTTG	GCCTGCCTGGTGATAATCTTT
ChIRP		
BRCA1-CISAL (-1627,-1606)	CTAGACATAAAAGTTTTCCAAGTCCC	ACAGGGCAAGGCTCAGGACC
BRCA1-CISAL (-103,-94)	AGGGCAGGCACTTTATGGC	TACGAAATCAAGGTACAATCAGAGG

BRCA1(distal)	TTTGTTCGTTCCTCCCGTCT	CTCTGGTCTCCTTCCACGCT
GAPDH(proximal)	GACCTTCTTGCCTTGCTCTTG	GCCTGCCTGGTGATAATCTTT
GAPDH(distal)	TCCCCAATTTCATTCCCTTTA	CGCAGATGCCACGGATTAGTT

5' RACE	Sequence (5'-3')
UPM (10×) Primer	CTAATACGACTCACTATAGGGCAAGCAGTGGTATCAACGCAGAGT
RACE assay-outer	CCACCAGCGCCGTGACAACTGAC
UPS (10 μM) Primer	CTAATACGACTCACTATAGGGC
RACE assay-inner	CAGCCTGCACTGCTTGACACACTC

3' RACE	Sequence (5'-3')
3' Outer Primer	TACCGTCGTTCCACTAGTGATTT
RACE assay-outer	AAGTGACTCTTCCTTAGCTAAGAG
3' Inner Primer	CGCGGATCCTCCACTAGTGATTTCACTATAGG
RACE assay-inner	ATCCGCAGTTCCCAGGAATTCGC

Table S5. Sequences of shRNAs/siRNAs and probes used in this study. Related to Figure 3

	Sequence(5'-3')
CISAL shRNA	
shRNA #1	CCAATGCACGAAACCGAAA
shRNA #2	TGGCTATGGAATTGGAAGA
shRNA #3	TTGCACTAAGAGAAGAAAT
shRNA #4	CTCCTGAATTCGTCTCAAA
shRNA #5	CCTACTGACACTACCCTTA
shControl	TCTTAATCGCGTATAAGGC
GABPA siRNA	
siGABPA1	GGAGCTGATAGAAATTGAGATTGAT
siGABPA2	GCAGAGTGCACAGAAGAAAGCATTG
RNA oligonucleotides	
Oligo #1	AGAGCCAGACGGACUCCAUC
Oligo #2	ACUCCAUCGUGACUCCUUCA
Oligo #3	CUCCUUCACUCGCAGCCCCU
Oligo #4	CAGCCCCUUACCCACCCCCU
Oligo #5	CACCCCCUUCCUCAAGGACU
Oligo-wt	GGACUCCAUCGUGACUCCUUCACUCGCAGCCCCU UACCCACCCCCUUCCUCAAGGACUUAACUUGUGC
Oligo-mut	GGACUCCAUCGUGACUCCUUCAAGACAUCAGAGG AUGAGUGCCCCUUCCUCAAGGACUUAACUUGUGC
ChIRP probes	
ChIRP #1	GTGTCAGTAGGAATCTTGGT
ChIRP #2	GAAGCCTCACATCATTAAGC
ChIRP #3	AGTCTATCCTAAGGTGATGG
ChIRP #4	GAACTGGTGCAAAGAATGAC
ChIRP #5	AAAGAATGCCTGTGTTTCGA
ChIRP #6	TCATCCTGTTCTCATGCTAA
ChIRP #7	TGCTGACATTACACGATTTC
ChIRP #8	GGCATAAAGGACTCACTTCT

ChIRP #9	GGCTGGGTATGTTACTCATT
Random probe	TGGGAGTGTTTATACGCGTA
In situ hybridization (ISH)	
CISAL	TAAGCTTCAGTCAGGCAGGCAT
Scramble	GTGTAACACGTCTATACGCCCA
U6	CACGAATTTGCGTGTCATCCTT
β-actin	CTCATTGTAGAAGGTGGGTGCCA

Transparent Methods

Cell culture

Two human TSCC cell lines, CAL-27 and SCC-9, were obtained from the American Type Culture Collection. CAL-27 cells were cultured in Dulbecco's modified Eagle's medium (Gibco, Rockville, MD, USA) supplemented with 10% fetal bovine serum (Invitrogen, Carlsbad, CA, USA). SCC-9 cells were cultured in Dulbecco's modified Eagle's medium-F12 (Gibco) supplemented with 10% fetal bovine serum. Cells were cultured at 37°C in a humidified atmosphere containing 5% CO2. For drug treatment, cisplatin (Sigma, USA), adriamycin (ADR) (Sigma, USA) or camptothecin (CPT) (Sigma, USA) were administered at a dose corresponding to their IC50(Fan et al., 2015a; Fan et al., 2015b) for 2 h, while 5-aza-2′-deoxycytidine (5-aza-dC) (Sigma, A3656) and trichostatin A (TSA) (Sigma, T8552) were administered for 72 h at 100 ng/mL(Wei et al., 2005) and the medium was changed every 24 h.

Electrophoretic mobility shift assay (EMSA)

EMSA was performed as previously described with slight modifications(Schmitz et al., 2010). Briefly, a total of 0.5 pmoles of a biotin-labeled DNA fragment (BRCA1-70, from -1655 to -1586; BRCA1-120, from -1685 to -1566) was obtained by PCR and incubated with 10 pmoles of synthetic RNA oligonucleotides (Table S 5) in 10 mM Tris-HCl (pH 7.4), 25 mM NaCl, 10 mM MgCl$_2$, and 10% glycerol for 2 h at room temperature. Then, 30 U of RNase H (Invitrogen™, 18021071) or RNase A (Thermo Scientific™, R1253) was used to test the resistance of DNA:RNA triplexes to RNase digestion. Triplex formation was monitored by electrophoresis on 8% polyacrylamide gels, followed by transfer to a nylon membrane and development using the BrightStar® BioDetect™ Kit System (Ambion).

Chromatin immunoprecipitation (ChIP)

ChIP assays were performed as previously described(Fan et al., 2015b). Briefly, CAL-27 cells (5×10^6) were washed with PBS and incubated for 10 min with 1% formaldehyde at room temperature. Crosslinking was halted with 0.1 M glycine for 5 min. The cells were washed twice with PBS and lysed for 1 h at 4°C in a lysis buffer, then sonicated into chromatin fragments with an average length of 500-800 bp, as accessed via agarose gel electrophoresis. The samples were precleared with Protein-A agarose (Roche) for 1 h at 4°C on a rocking platform. Then, 5 μg of specific antibodies was added and the samples rocked overnight at 4°C. Immunoprecipitated DNA was purified using the QIAquick PCR purification kit (Qiagen) according to the

manufacturer's protocol. The final ChIP DNA was then used as a template in qPCR with the primers in Table S 4. ChIP-grade anti-RNA polymerase II antibody (Abcam, ab5131), anti-GABPA antibody (Millipore, ABE1047), anti-pan methylated lysine antibody (Abcam, ab7315), anti-histone H3 (tri methyl K4) antibody (Abcam, ab8580), anti-acetylated histone H3 (Abcam, ab47915), anti-acetylated histone H4 (Millipore, 06–866), anti-GAL4(DNA binding domain) antibody (Millipore, 06-262), and anti-IgG (Sigma, I5006) were used in this study.

Chromatin isolation by RNA purification (ChIRP)

ChIRP assays were performed as previously described with slight modifications(Chu et al., 2012). Briefly, ChIRP probes (3'-end biotin labeled) against CISAL and the random probe were designed and synthesized by RiboBio (Guangzhou, China). CAL-27 cells were fixed with 1% glutaraldehyde for 10 min. The crosslinked cells were lysed with lysis buffer (50 mM Tris-Cl, pH 7.5, 10 mM EDTA, 1% SDS protease inhibitors and SUPERase-In). The lysates were sonicated by Bioruptor (Diagenode, Denville, USA) at 4 ℃ on the setting with pulse intervals of 30 seconds ON and 45 seconds OFF for a total of 30 min. The sonicated cell lysates were hybridized with a mixture of biotinylated DNA probes against human CISAL in hybridization buffer (50 mM Tris-Cl pH 7.5, 750 mM NaCl, 1% SDS, 1 mM EDTA, 15% formamide, protease inhibitors and SUPERase-In) overnight at 4℃. Then, the binding complexes were recovered by streptavidin-conjugated C1 magnetic beads (Invitrogen, Waltham, USA), and DNA was eluted with elution buffer (50 mM NaHCO$_3$, 1% SDS). Quantitative PCR was performed to detect the enrichment of specific regulatory regions associated with CISAL, and the percentage enrichment of the locus over the input DNA was determined.

RNA pull down assay

Full-length CISAL and antisense CISAL sequences were prepared by in vitro transcription using TranscriptAid T7 High Yield Transcription Kit(Thermo Scientific, K0441) and treated with RNase-free DNase I and purified with GeneJET RNA purification kit(Thermo Scientific, K0731). Nuclear extracts were prepared with NE-PER Nuclear Protein Extraction Kit (Thermo Scientific, 78833). For *in vitro* translated protein, full length of ORF fragment of a specific gene was inserted into pcDNA3.1 and was *in vitro* transcribed and translated with 1-Step Human Coupled *In Vitro* Expression Kit (Thermo Scientific, 88881) following standard protocols. RNA

pull down assay was performed with Magnetic RNA-Protein Pull-Down Kit (Pierce, 20164) according to manufacturer's instructions. Three micrograms of biotin-labeled RNA and 1 mg of nuclear extract were used in each pull down assay. The retrieved protein was detected with standard immunoblot technique.

RNA immunoprecipitation (RIP)

RIP was performed using a Magna RIP RNA-Binding Protein Immunoprecipitation Kit (Millipore, 17-700) according to the manufacturer's instructions. Briefly, 1×10^7 cells were harvested and lysed with RIP lysis buffer for 20 min at 4°C. When the cell extract was removed from the dish, it was centrifuged for 15 min at 12000 g and 4°C. The supernatant was divided into two parts, and then, anti-GABPA antibody (Millipore, ABE1047) and IgG were added, followed by rotation at 20 rpm for 1 h. Protein beads were added to each tube followed by rotation at 20 rpm for 0.5 h. A magnetic frame was applied to remove the supernatant, followed by three washes with a lysis buffer. Protease K and RNase inhibitor were added to the lysis buffer, followed by rotation for 30 min at 55°C to remove the protein. TRIzol LS was added to the remaining solution, and RNA was then extracted from it. qRT-PCR was applied to assess CISAL expression in the immunocomplex.

***BoxB*-λN tethering assay**

As previously described(Wang et al., 2011b), the *BoxB* tethering system uses viral RNA–protein interactions, in which *BoxB* (GGGCCCUGAAGAAGGGCCC) is a viral RNA that can be recognized and bound by the viral anti-terminator protein λN (1-22: MDAQTRRRERRAEKQAKWKAAN). Fusion of CISAL with *BoxB* enables the fused CISAL-*BoxB* to be bound by λN. Subsequently, λN protein is fused with the DNA-binding domain (DBD) of GAL4, which in turn recognizes UAS (CGGAGTACTGTCCTCCG) sites on the reporter plasmid DNA. Using this technique, CISAL-*BoxB* can be tethered to the 5×UAS sites on a reporter plasmid with the help of the λN–GAL4 fusion protein. The 5×*BoxB* DNA fragment with 5-ATATA-3 linking each other was synthesized from Generay Biotech (Shanghai, China). CISAL-*BoxB* was obtained by substituting the BRCA1 binding site in CISAL lncRNA with 5×*BoxB* using overlap PCR and cloned into a pcDNA3.1. The CISAL binding site in BRCA1 promoter cloned into pGL4.20 luciferase reporter vector was substituted with 5×UAS fragment to get pGL4-BRCA1-UAS using Q5 Site-Directed Mutagenesis Kit (NEB, Catalog # E0552). The GABPA recognizing site in pGL4-BRCA1-UAS was mutated to get pGL4-BRCA1-UAS-GABPA-mut.

Luciferase assay

A luciferase assay was carried out as previously described with modifications(Fan et al., 2015a). Briefly, pGL4-BRCA1-wt was obtained by cloning a 2200 bp DNA fragment (-2000 to +200 with respect to the BRCA1 transcriptional starting site) into the pGL4.20 vector upstream of the luciferase reporter gene. The mutant pGL4-BRCA1-mut plasmid was obtained by mutating the predicted CISAL binding motif. pGL4-BRCA1-GABPA-mut was generated by mutating the GABPA recognizing motif. MFF expression cassette containing miR-593-5p targeting site (wild type or mutated) was cloned into the pGL3-control plasmid downstream of the luciferase reporter gene, as previously described(Fan et al., 2015b). These pGL4.20 derivated reporter vectors were transfected into CAL-27 cells and the stable cell lines were obtained through puromycin selection for two weeks. CAL-27 cells stably expressing pGL4-BRCA1-wt or pGL4-BRCA1-mut were transfected with CISAL overexpressing vector or siRNAs using Lipofectamine 3000 (Invitrogen, Carlsbad, CA, USA). The pRL-TK plasmid delivering Renilla Luciferase was co-transfected as a control. The luciferase activities were measured using a Dual Luciferase Reporter Assay Kit (Promega, Madison, WI, USA), and the target effect was presented as the luciferase activity of the reporter vector with the target sequence relative to that without the target sequence.

Mitochondrial staining and analysis of mitochondrial fission

Mitochondrial staining was performed as described previously by us and other researchers with some modifications(Fan et al., 2015a; Fan et al., 2015b; Wang et al., 2011a). Briefly, cells were plated onto coverslips and treated as previously described. Then, the cells were stained for 30 min with 0.1 μM MitoTracker Red CMXRos (Molecular Probes). The mitochondria were visualized using a laser scanning confocal TCS SP5 microscope (Leica, Solms, Germany), and the mitochondrial morphology was assessed and quantified as described previously (Tanaka and Youle, 2008).

LncRNA expression profiles

CAL-27 and SCC-9 cells were treated with cisplatin (Sigma, USA) at its IC50(Fan et al., 2015a; Fan et al., 2015b) for 24 h for lncRNA microarray assays. Sample labeling and array hybridization were performed by Arraystar Human lncRNA Microarray V3.0 according to the Arraystar microarray-based gene expression analysis protocol.

mRNA profiles

CAL-27 and SCC-9 cells stably transduced with shRNA targeting CISAL were treated with cisplatin at the IC50 (Sigma, USA) for 24 h for mRNA profiling. The microarray data sets were normalized in GeneSpring GX using the Agilent FE one-color scenario.

Rapid amplification of cDNA ends (RACE)

RACE experiments were performed using the Smart RACE CDNA Amplification Kit (Clontech, Mountain View, CA) according to the manufacturer's instructions. Briefly, at least two sets of primers were designed and synthesized for nested PCR. The RACE PCR products were confirmed and separated by electrophoresis using a 1.5% agarose gel. Then, the amplified bands were sequenced. The CISAL sequence from the RACE analyses is listed in Supplementary Table 2. The gene-specific primers used for the nested PCR step of the RACE analysis of CISAL are listed in Supplementary Table 4.

RNA isolation and quantitative real-time PCR (qRT-PCR)

Total RNA was extracted using TRIzol reagent (Invitrogen, Waltham, MA, USA), and both nuclear and cytoplasmic RNA was isolated and purified with an RNA Purification Kit (Norgen, 21000-NB). cDNA was synthesized using M-MLV reverse transcriptase (Invitrogen, Waltham, MA, USA) according to the manufacturer's instructions (Invitrogen, Waltham, MA, USA). Then, qRT-PCR was performed using SYBR Green Real-time PCR Master Mix (ReverTra Ace, Toyobo) and a LightCycler 480 (Roche, Basel, Switzerland) according to the manufacturer's instructions. The PCR primers are listed in Supplementary Table 4. Ct values were calculated using the LightCycler 480 (Roche, Basel, Switzerland). The primers for hsa-miR-593-5p and U6 were purchased from RiboBio (Guangzhou, China).

Transfections

BRCA1 shRNAs (TRCN0000244987 and TRCN0000244986) were purchased from Sigma-Aldrich (St. Louis, USA), and scramble shRNA (#1864) was obtained from Addgene (MA, USA). GABPA Stealth Interference RNAs were purchased from Thermo Fisher Scientific. Sequences for these siRNAs are listed in Supplementary Table 5. Cells were plated in 6-well plates and transfected using Lipofectamine 3000 (Invitrogen, Waltham, MA, USA) according to the manufacturer's instructions.

Plasmid construction and establishment of stable cell lines

GABPA was amplified from cDNA using primers (Supplementary Table 4) and cloned into a pcDNA3.1 plasmid. Human full length BRCA1 was amplified from SFB-BRCA1 plasmid (#99394) purchased from Addgene (MA, USA) and cloned into

a pcDNA3.1 plasmid. DNA fragments (BRCA1-70 and BRCA1-120), including the complementary sequence to the predicted CISAL binding sites at (1134, 1157), were amplified from the plasmid delivering the BRCA1 promoter and then labeled with biotin using the Biotin 3' End DNA Labeling Kit (Thermo Fisher Scientific, #89818) according to the manufacturer's instructions. The primers used to amplify these DNA fragments are listed in Supplementary Table 4. The full length CISAL was amplified from cDNA using primers and cloned into a pcDNA3.1. The site of CISAL binding to BRCA1 promoter was mutated to get mut-CISAL. A series 5' deletion mutants (1-1300, 1-1100, 1-900, 1-700, 1-500, 1-300) and antisense of CISAL were amplified from wt-CISAL and cloned into a pcDNA3.1. All site-specific mutants were obtained using the QuikChange II Site-Directed Mutageneration Kit (Agilent, Catalog #200523). shRNAs targeting CISAL were constructed using the pSIREN-RetroQ-DsRed-Express retrovirus vector from Takara Biotechnology (Dalian, China). The CISAL siRNA target sequences and control sequences are listed in Supplementary Table 5. To generate stable TSCC cell lines with CISAL knockdown or overexpression, pSIREN-RetroQ-DsRed-Express or pBABE-puro based construct was co-transfected with helper plasmids into HEK293T cells to produce recombinant viruses. Infection and screening of TSCC stable cells were performed as we have described previously(Fan et al., 2015a; Fan et al., 2015b).

Bioinformatic analysis

Three different methods including open reading frame finder from NCBI (Kozak strength)(Nishikawa et al., 2000), txCdsPredict from UCSC and phyloCSF(Lin et al., 2011) were performed to calculate the coding potential of CISAL. Defining txCdsPredict: 800(Prensner et al., 2011) as thresholds, the scores of open reading frames from CISAL were well below the thresholds as indicating as txCdsPredict scores=285. Non coding frame was detected by phyloCSF(Cabili et al., 2011) as scores≤0.

The potential binding sites between CISAL and BRCA1 or GAPDH were predicted by IntaRNA (http://rna.informatik.uni-freiburg.de/IntaRNA/Input.jsp). The base-pairing energy for an RNA/RNA duplex model of seed-based regions along the CISAL transcript and 2,000 bp upstream and 200 bp downstream of the TSS of BRCA1 or GAPDH was calculated(Grote et al., 2013). The duplex energy was computed for each such region and displayed in a heatmap. The probabilities were then averaged for a sliding window of seed-based regions to give the average RNA

accessibility of the binding region. The average probability of single-stranded RNA was computed using a Sfold server (http://sfold.wadsworth.org)(Ding et al., 2004).

Entrez cancer gene list was established as previously described(Domazet-Loso and Tautz, 2010). Cancer associated TFs were defined by overlapping Entrez cancer genes and TFs with ChIP-seqs in Encyclopedia of DNA Elements (ENCODE). We chose TFs ChIP-seqs from GM12878, K562, HepG2 and Hela-S3 cell lines and downloaded them from ENCODE. We then processed them by ENCODE processing pipeline and the TFs binding sites at BRCA1 promoter (NG_056086.1) were analyzed. To predict the potential GABPA binding site at BRCA promoter region, we used motif-counter (https://bio.tools/motifcounter) to scan BRCA promoter region both strand with GABPA motif which was downloaded from JASPAR database.

Northern blotting

Northern blots were performed as previously reported with some modifications(Kim et al., 2016; Nakamura et al., 2001). Briefly, 10 μg of RNA was fractionated on a 1% agarose gel at 50 V for 1.5 h. The RNA was then transferred to a nitrocellulose membrane (Millipore, HATE00010) overnight for at least 16 h. After being washed with 2× SSC, the nitrocellulose membrane was UV crosslinked at 1,000 μF and prehybridized for 30 min at 52°C in UltraHyb buffer (Roche, 11796895001). Then, DIG-labeled probes were added, and the blots were hybridized in 10 mL of UltraHyb buffer. After being washed for 2×5 min at the hybridization temperature in low-stringency buffer and for 2×15 min at the hybridization temperature in high-stringency buffer, the blots were incubated for 30 min in blocking solution and then for 30 min in anti-digoxigenin-AP solution and analyzed on a phosphorimager (Molecular Dynamics) with a CSPD detection buffer.

RNA fluorescence in situ hybridization (FISH)

Cells were washed with PBS and fixed with 4% formaldehyde in PBS (pH 7.4) for 20 min at room temperature. Then, the cells were permeabilized in PBS containing 0.1% Triton X-100 at room temperature for 15 min, washed with PBS for 3×5 min, digested with 0.05% trypsin, and subjected to dehydration in an ethanol series (75%, 85% and 100%) prior to hybridization. Hybridization was performed using a DIG-labeled CISAL probe in hybridization solution (probe dilution 1:1000) (Exiqon, Denmark) for 16 h at 52°C in a humidified chamber. Next, the cells were washed for 30 min in 2× SSC at 52°C and then for 30 min in 25% deionized formamide/2× SSC at 52°C. Cells on coverslips were counterstained with DAPI and imaged using a TCS SP5 confocal

microscope (Lecia, Solms, Germany).

Western blotting

Immunoblotting was performed as previously described (Fan et al., 2015a). Briefly, cells were lysed for 0.5 h at 4°C in RIPA Buffer (R0278, Sigma) containing a protease inhibitor cocktail. Protein extracts were resolved through 8% SDS-polyacrylamide gel electrophoresis; transferred to polyvinylidene difluoride membranes (BioRad, Berkeley, CA, USA); probed with antibodies against human MFF (ab81127, Abcam), BRCA1 (ab191042, Abcam), GABPA (Millipore, ABE1047), PCNA (ab92552, Abcam) and β-actin (Proteintech, Chicago, IL, USA) and then with a peroxidase-conjugated secondary antibody (Proteintech); and finally visualized via chemiluminescence (GE, Fairfield, CT, USA).

Immunofluorescence staining

Cells on coverslips were stained for mitochondria and cytochrome c(CYT c). After mitochondrial staining, the cells were incubated with primary antibodies against CYT c (Santa Cruz, sc-13560) and then incubated with FITC-conjugated secondary antibodies (Invitrogen). The coverslips were counterstained with 46-diamidino-2-phenyl indole and imaged under a confocal microscope TCS SP5 (Lecia, Solms, Germany).

Apoptosis assay

For apoptosis assays, CAL-27 and SCC-9 cells were treated with cisplatin under 8×10^{-6} and 1.8×10^{-5} M (Sigma, USA) for 24 h(Fan et al., 2015a). Apoptosis was detected using TUNEL, flow cytometry and caspase-3/7 activity assays. TUNEL assays were performed using a kit from Roche (Cat. No. 11684795910) according to the user's instructions. Sections were examined with an ImagerZ1 microscope (Zeiss, Jena, Germany). An investigator blinded to the treatment quantified 20 random fields from the samples. Flow cytometry was performed using Annexin V and propidium iodide double staining (Sigma-Aldrich). Caspase-3/7 activity was determined using an Apo-ONE® Homogeneous Caspase-3/7 Assay Kit from Promega according to the manufacturer's protocol.

In situ hybridization (ISH)

In situ hybridization was performed as previously described(Fan et al., 2015a) according to the manufacturer's protocol (Exiqon, Vedbaek, Denmark). Briefly, after demasking, CISAL was hybridized to 5'DIG-labeled CISAL probes. Then, DIG was recognized via a specific anti-DIG antibody directly conjugated to alkaline

phosphatase. The nuclei were counterstained with Kernechtrot Solution (N3020, Sigma). In all, 5×200 tumor cells were counted randomly in each section. Sections with more than 300 RNA-positive cells were considered to have high expression.

Immunohistochemistry (IHC)

Immunohistochemistry was performed as described previously(Fan et al., 2015a). Briefly, slice of paraffin-embedded tissues were deparaffinized, rehydrated and subjected to antigen retrieval. Then, the tissues were incubated with anti-BRCA1 (ab16780, Abcam) antibody at 4 °C overnight and then successively incubated with secondary antibody and streptavidin–horseradish peroxidase complex. Diaminobenzidine (Dako, Carpinteria, CA, USA) was used as a chromogen, and the nuclei were counterstained with hematoxylin. In total, 5×200 tumor cells were counted in each section. Sections with more than 300 BRCA1-positive cells were considered to have high BRCA1 expression.

Tumor xenografts

Male BALB/c nude mice aged 4 to 6 weeks were prepared for tumor implantation. CAL-27 cells ($5×10^6$/mouse) stably expressing CISAL or shRNA targeting CISAL were resuspended in 150 μL of PBS and injected subcutaneously into the flanks of the nude mice. One week after implantation, when the tumor became palpable at ~2 mm in diameter, either cisplatin or saline were intraperitoneally injected at 5 mg/kg body weight every three days from days 8 to 32. Tumor volume was calculated beginning at the first day of cisplatin injection using the formula TV (mm^3)=length×width^2×0.5. At day 35, the primary tumors were carefully removed for analysis as indicated.

Patient and tissue samples

Fresh tumor tissues from 29 TSCC patients for identification of lncRNA profiles were obtained before and after neoadjuvant chemotherapy while specimens from 113 locally advanced TSCC patients were obtained before neoadjuvant chemotherapy between Jan 1, 2004, and Dec 31, 2010. Patients with locally advanced resectable TSCC (stage III or IVA) underwent one or two cycles of neoadjuvant chemotherapy(Zhong et al., 2013) (75 mg/m^2 cisplatin on day 1, 75 mg/m^2 docetaxel on day 1, and 750 mg/m^2 fluorouracil on days 1 to 5), and the tumor response to neoadjuvant chemotherapy was assessed by CT/MRI studies prior to radical resection. According to the Response Evaluation Criteria in Solid Tumors of the World Health Organization, TSCC patients with progressive or stable disease were characterized as having nonsensitive TSCC, whereas those who showed a partial or complete response

were determined to have cisplatin-sensitive TSCC. Surgery was performed at least 2 weeks after the completion of neoadjuvant chemotherapy. Histological diagnoses and scoring of all the cases were performed by two independent pathologists. The survival time was calculated from the date of surgery to the date of death or last follow-up. The date of death was obtained from patient records or through follow-up telephone calls.

Study approval

Ethical consent was given by the Sun Yat-sen University Committee for Ethical Review of Research Involving Human Subjects. Human TSCC were obtained with written and informed consent under 2014114 from Sun Yat-sen Memorial Hospital. The animal experiments were in accordance with the institutional authorities' guidelines and formally approved by the Animal Ethics Committee of Sun Yat-sen University.

Statistics

All data are presented as mean ± SEM. Comparisons between 2 groups were done by 2-tailed Student's t tests using the SPSS 18.0 package (SPSS, Chicago, IL, USA). For multiple comparisons between groups, 1-way ANOVA followed by Dunnett's multiple comparisons tests was performed. A chi-square test were used to analyze the relationship between CISAL and BRCA1 expression and the clinicopathological characteristics using the SPSS 18.0 package. To measure associations between pairs of variables, Spearman order correlations were performed. Kaplan-Meier survival curves were plotted, and a log-rank test was performed. At least three independent experiments were performed for all cell culture experiments. Throughout the study, P values below 0.05 were considered significant.

Data availability

Data have been deposited in the Gene Expression Omnibus (GEO) DataSets (https://www.ncbi.nlm.nih.gov/gds) under the following accession numbers: GSE114929 and GSE115116.

Supplemental Reference

Cabili, M.N., Trapnell, C., Goff, L., Koziol, M., Tazon-Vega, B., Regev, A., and Rinn, J.L. (2011). Integrative annotation of human large intergenic noncoding RNAs reveals global properties and specific subclasses. Genes & development *25*, 1915-1927.

Chu, C., Quinn, J., and Chang, H.Y. (2012). Chromatin isolation by RNA purification (ChIRP). Journal of visualized experiments : JoVE.

Ding, Y., Chan, C.Y., and Lawrence, C.E. (2004). Sfold web server for statistical folding and rational design of nucleic acids. Nucleic acids research *32*, W135-141.

Domazet-Loso, T., and Tautz, D. (2010). Phylostratigraphic tracking of cancer genes suggests a link to the emergence of multicellularity in metazoa. BMC biology *8*, 66.

Fan, S., Chen, W.X., Lv, X.B., Tang, Q.L., Sun, L.J., Liu, B.D., Zhong, J.L., Lin, Z.Y., Wang, Y.Y., Li, Q.X.*, et al.* (2015a). miR-483-5p determines mitochondrial fission and cisplatin sensitivity in tongue squamous cell carcinoma by targeting FIS1. Cancer letters *362*, 183-191.

Fan, S., Liu, B., Sun, L., Lv, X.B., Lin, Z., Chen, W., Chen, W., Tang, Q., Wang, Y., Su, Y.*, et al.* (2015b). Mitochondrial fission determines cisplatin sensitivity in tongue squamous cell carcinoma through the BRCA1-miR-593-5p-MFF axis. Oncotarget *6*, 14885-14904.

Grote, P., Wittler, L., Hendrix, D., Koch, F., Wahrisch, S., Beisaw, A., Macura, K., Blass, G., Kellis, M., Werber, M.*, et al.* (2013). The tissue-specific lncRNA Fendrr is an essential regulator of heart and body wall development in the mouse. Developmental cell *24*, 206-214.

Kim, Y.K., Kim, B., and Kim, V.N. (2016). Re-evaluation of the roles of DROSHA, Export in 5, and DICER in microRNA biogenesis. Proceedings of the National Academy of Sciences of the United States of America *113*, E1881-1889.

Lin, M.F., Jungreis, I., and Kellis, M. (2011). PhyloCSF: a comparative genomics method to distinguish protein coding and non-coding regions. Bioinformatics *27*, i275-282.

Nakamura, K., Robertson, M., Liu, G., Dickie, P., Nakamura, K., Guo, J.Q., Duff, H.J., Opas, M., Kavanagh, K., and Michalak, M. (2001). Complete heart block and sudden death in mice overexpressing calreticulin. The Journal of clinical investigation *107*, 1245-1253.

Nishikawa, T., Ota, T., and Isogai, T. (2000). Prediction whether a human cDNA sequence contains initiation codon by combining statistical information and similarity

with protein sequences. Bioinformatics *16*, 960-967.

Prensner, J.R., Iyer, M.K., Balbin, O.A., Dhanasekaran, S.M., Cao, Q., Brenner, J.C., Laxman, B., Asangani, I.A., Grasso, C.S., Kominsky, H.D*., et al.* (2011). Transcriptome sequencing across a prostate cancer cohort identifies PCAT-1, an unannotated lincRNA implicated in disease progression. Nature biotechnology *29*, 742-749.

Schmitz, K.M., Mayer, C., Postepska, A., and Grummt, I. (2010). Interaction of noncoding RNA with the rDNA promoter mediates recruitment of DNMT3b and silencing of rRNA genes. Genes & development *24*, 2264-2269.

Tanaka, A., and Youle, R.J. (2008). A chemical inhibitor of DRP1 uncouples mitochondrial fission and apoptosis. Molecular cell *29*, 409-410.

Wang, J.X., Jiao, J.Q., Li, Q., Long, B., Wang, K., Liu, J.P., Li, Y.R., and Li, P.F. (2011a). miR-499 regulates mitochondrial dynamics by targeting calcineurin and dynamin-related protein-1. Nature medicine *17*, 71-78.

Wang, K.C., Yang, Y.W., Liu, B., Sanyal, A., Corces-Zimmerman, R., Chen, Y., Lajoie, B.R., Protacio, A., Flynn, R.A., Gupta, R.A*., et al.* (2011b). A long noncoding RNA maintains active chromatin to coordinate homeotic gene expression. Nature *472*, 120-124.

Wei, M., Grushko, T.A., Dignam, J., Hagos, F., Nanda, R., Sveen, L., Xu, J., Fackenthal, J., Tretiakova, M., Das, S*., et al.* (2005). BRCA1 promoter methylation in sporadic breast cancer is associated with reduced BRCA1 copy number and chromosome 17 aneusomy. Cancer research *65*, 10692-10699.

Zhong, L.P., Zhang, C.P., Ren, G.X., Guo, W., William, W.N., Jr., Sun, J., Zhu, H.G., Tu, W.Y., Li, J., Cai, Y.L*., et al.* (2013). Randomized phase III trial of induction chemotherapy with docetaxel, cisplatin, and fluorouracil followed by surgery versus up-front surgery in locally advanced resectable oral squamous cell carcinoma. Journal of clinical oncology : official journal of the American Society of Clinical Oncology *31*, 744-751.